Ministry of Higher Education and Scientific Research

Kasdi Merbah Ouargla University

Faculty of New Information and Communication Technologies

Dissertation

ACADEMIC MASTER

Domain: Sciences and Technologies

Branch: Telecommunications

Speciality "Systems of telecommunications"

A dual-band RF/microwave energy harvesting rectenna for Wi-Fi applications

Presented publicly by

HALIMI FATIMA YASMINE AND DEBIEB FATIMA ZOHRA KENZA

June 8, 2026

Jury

Hassiba LOUAZENE,	MCA at university of Ouargla	President
Hachemi CHENINA,	MCB at university of Ouargla	Examiner
Boualem MEKIMAH,	MCA at university of Ouargla	Supervisor
Abdelkrim BELHEDRI,	MCB at university of Ouargla	Co-Supervisor
Amira HAMIDI,	PhD at university of Ouargla	Guest

P
F
E

Dedications

Firstly, praise be to "ALLAH" for the blessing of access.

To my dear parents, who have always been the light that has guided my path and the cornerstone of my life, I dedicate this thesis with all my love and gratitude.

To my brothers and sisters, Arwa and Roufaida , my fellow travellers with whom I shared the hardships of study and the joy of success.

To my dear friends: D. Fatima Zohra Kenza, KH.Asma, B.Asma, L.Safa, H.Basma, and B.Nada. I am deeply grateful for the moments we shared and the cherished memories we created together. Thank you for being an irreplaceable part of this journey.

To my esteemed teachers, who never withheld their knowledge and guidance from us and who served as a beacon lighting up the darkness of ignorance for us.

I dedicate to you the fruit of my modest efforts, in gratitude and in recognition of every moment of support you have given me.

Halimi Fatima Yasmine

Dedications

First and foremost, all praise and gratitude are due to Allah, the Most Merciful and the Most Compassionate, for His endless mercy, love, and strength that guided me through every step of this journey. His presence gave me patience and courage to continue even when the path was difficult, and I am forever grateful for His blessings. I dedicate this achievement with all my heart to the most important people in my life:

To my beloved mother, Thank you for your love, support, and encouragement throughout my studies. Your prayers, sacrifices, and belief in me have helped me achieve this milestone. I am truly grateful for everything you have done for me. .

To my dear father, My first hero. Thank you for your sacrifices, hard work, and for always providing me with everything I needed and more. Your support has always been my strength, and I dedicate this achievement to you with deep gratitude.

To my brothers Nassim, Adel, Salah, and Chakib, You are my strength and support in every step of this journey. Thank you for always believing in me and standing by my side.

To my best friends Salsabil, Wiam, Maria, Lina and Ritedje, Thank you for your true friendship, support, and the comfort you gave me during difficult and stressful moments. I will always be grateful for you.

To my classmate F. Yasmine,

To all my teachers without exception, Thank you for your guidance and knowledge. Your teachings have been essential in shaping my academic journey.

Finally, this success is not only mine. It belongs to everyone who supported me, believed in me, and supported me with kindness and faith.

Thank you
DEBIEB Fatima Zohra Kenza

Acknowledgements

First and foremost, we express our utmost gratitude to Almighty 'ALLAH' for bestowing upon us the strength, perseverance, and faith required to successfully accomplish this research work and conclude our academic journey.

We extend our profound gratitude and sincere appreciation to our esteemed supervisor, Dr. Boualem Mekimah, MCA at the University of Ouargla, for his invaluable guidance, unwavering support, and continuous confidence in our capabilities. We are deeply privileged to have been part of his research team, and we highly value his insightful feedback and commitment to fostering a positive, stimulating, and productive academic environment. It has been a distinct honor and a privilege to work under his supervision.

We would like to express our deep gratitude to our co-supervisor, Dr. Abdelkrim BELHEDRI, MCB at the University of Ouargla, for his invaluable guidance throughout this research and for honoring us by serving on our defense committee. We highly appreciate his genuine interest in our work and his willingness to evaluate it, enriching this project with his constructive insights and extensive expertise.

We would also like to express our sincere gratitude to Dr. Hassiba Louazene, MCA at the University of Ouargla, for her genuine interest in our research and for granting us the distinct honor of presiding over our graduation thesis defense jury. We are highly privileged to benefit from her profound knowledge and extensive academic expertise.

We would also like to express our deep gratitude to Dr. Hachemi Chenina, MCB at the University of Ouargla, for honoring us by serving as an examiner on our defense committee. We highly appreciate his genuine interest in our research and his willingness to evaluate this work, enriching it with his constructive insights and extensive expertise.

We would also like to express our sincere gratitude to Ms. Amira HAMIDI, PHD at the University of Ouargla, for honoring us as a guest member of our defense jury. We highly appreciate her vital presence, her keen interest in our research, and her valuable dedication to evaluating and enriching this work with her profound academic expertise.

We would also like to extend our heartfelt gratitude to the entire faculty and staff of the Department of Electronics and Telecommunications at Kasdi Merbah Ouargla University (UKMO) for their dedication, invaluable instruction, and unwavering support. We are profoundly grateful for their patience, mentorship, and above all, their inspiring humility, which has left a lasting impression on us throughout our academic journey.

Finally, we owe a deep debt of gratitude to our families and friends for their unconditional love, patience, and endless support. We also extend our appreciation to everyone who, directly or indirectly, contributed to the successful completion of this research work.

Abstract

In this work, we propose a dual-band rectenna designed for Wi-Fi energy harvesting at 2.45 GHz and 5.8 GHz. The rectenna integrates a dual-band monopole antenna with a dual-band rectifier that employs a voltage doubler topology based on SMS7630 series Schottky diode. The proposed antenna, designed and optimized in CST Microwave Studio, covers the same frequency bands with gains of 1.75 dBi and 3.15 dBi, and radiation efficiencies of 84% and 91% at 2.45 GHz and 5.8 GHz, respectively. The rectifier circuit, developed using Keysight ADS simulator, achieves a peak power conversion efficiency (PCE) of 75% at 2.45 GHz and 50% at 5.8 GHz, with corresponding DC output voltages of 2.45 V and 2.1 V. These results demonstrate that the proposed rectenna is a promising candidate for efficient and reliable RF energy harvesting in Wi-Fi applications.

Keywords–Radio frequency (RF) energy harvesting, Rectenna, Wi-Fi bands, Impedance matching.

Résumé

Dans ce travail, nous proposons une rectenna bi-bande conçue pour la récupération d'énergie Wi-Fi à 2,45 GHz et 5,8 GHz. La rectenna intègre une antenne monopôle bi-bande et un redresseur bi-bande utilisant une topologie de doubleur de tension basée sur une diode Schottky de la série SMS7630. L'antenne proposée, conçue et optimisée dans CST Microwave Studio, couvre les mêmes bandes de fréquences avec des gains de 1,75 dBi et 3,15 dBi, et des rendements de rayonnement de 84% et 91% à 2,45 GHz et 5,8 GHz, respectivement. Le circuit redresseur, développé à l'aide du simulateur ADS de Keysight, atteint un rendement de conversion de puissance (PCE) maximal de 75% à 2,45 GHz et de 50% à 5,8 GHz, avec des tensions de sortie en courant continu correspondantes de 2,45 V et 2,1 V. Ces résultats démontrent que la rectenna proposée est une candidate prometteuse pour une récupération d'énergie RF efficace et fiable dans les applications Wi-Fi.

Mots clés–Récupération d'énergie par radiofréquence (RF), rectenna, bandes Wi-Fi, adaptation d'impédance.

ملخص

نُقدّم في هذا العمل هوائيًا لاقطًا ومقوّمًا ثنائي الحزمة، مُصمّمًا لحصاد طاقة الشبكات اللاسلكية عند الترددين 2.45 ~ جيجاهرتز و 5.8 ~ جيجاهرتز.

يدمج الهوائي المقترح بين هوائي أحادي القطب ثنائي الحزمة، ومقوّم ثنائي الحزمة يعتمد على بنية مضاعف الجهد باستخدام صمام شوتكي الثنائي

يغطي الهوائي المقترح الذي صُمم وحُسّن باستخدام برنامج محاكاة الكهرومغناطيسية ثلاثي الأبعاد نطاقي التردد المذكورين، محققًا كسبًا يبلغ 1.75 ديسيبل و 3.15 ديسيبل ، وكفاءة إشعاعية تصل إلى 84% و 91% عند الترددين 2.45 ~ جيجاهرتز و 5.8 ~ جيجاهرتز على التوالي.

أما دائرة المقوّم، التي طُوّرت باستخدام برنامج محاكاة الدوائر الإلكترونية المتقدمة، فقد حققت ذروة كفاءة تحويل طاقة بلغت 75% عند التردد 2.45 ~ جيجاهرتز و 50% عند التردد 5.8 ~ جيجاهرتز، مع جهد خرج مستمر مصاحب يبلغ 2.45 فولت و 2.1 فولت.

وتُثبت هذه النتائج أن الهوائي اللاقط والمقوّم المقترح يُعدّ خيارًا واعدًا لحصاد طاقة الترددات الراديوية بكفاءة وموثوقية في تطبيقات الشبكات اللاسلكية.

الكلمات المفتاحية هوائي لاقط .مقوم ثنائي الحزمة.دائرة المقوم.صمام شوتكي

Contents

Dedications ii

Dedications iii

Acknowledgements v

Summary ix

Contents x

List of Figures xiii

List of Tables xv

List of Acronyms and Abbreviations xvi

List of symbols xvii

General Introduction 1

1 General context of antennas 5

1.1 Introduction 6

1.2 Antennas classification 6

1.2.1 Wire antennas 6

1.2.2 Aperture antennas 7

1.2.3 Printed antennas 7

1.2.4 Optics based antennas 8

1.3 Antenna parameters 8

1.3.1 Electrical parameters 9

1.3.1.1 Input impedance 9

1.3.1.2 Reflection coefficient and the standing wave ratio 10

1.3.1.3 Frequency bandwidth 11

1.3.1.4 Quality factor . . . 12
1.3.2 Radiation parameters . . . 13
1.3.2.1 Radiation pattern . . . 13
1.3.2.2 Radiation characteristic function . . . 13
1.3.2.3 Half-Power Beamwidth . . . 15
1.3.2.4 Field polarization . . . 15
1.3.2.5 Field regions . . . 19
1.3.2.6 Antenna directivity . . . 20
1.3.2.7 Antenna gain . . . 20
1.3.2.8 Radiation efficiency . . . 21
1.3.2.9 Friis Transmission Equation . . . 21
1.4 Patch antenna . . . 22
1.4.1 Overall . . . 22
1.4.2 Basic patch antenna design . . . 22
1.4.3 Dielectric materials . . . 23
1.4.4 Conductive materials . . . 24
1.5 Feeding techniques for patch antennas . . . 24
1.5.1 Coaxial probe feeding . . . 24
1.5.2 Micro-strip line feed . . . 25
1.5.2.1 Aperture coupled feed . . . 25
1.5.2.2 Proximity coupling . . . 26
1.6 Conclusion . . . 27

2 RF and microwave energy harvesting systems 28
2.1 Introduction . . . 29
2.2 RF Energy Harvesting . . . 29
2.2.1 Description . . . 29
2.2.2 RF energy sources . . . 30
2.2.2.1 Energy harvesting from wi-Fi sources . . . 30
2.2.2.2 Mobile bases station/GSM/cellular sources . . . 30
2.2.2.3 TV and DTV sources . . . 31
2.2.3 Rectifier circuit . . . 31
2.2.3.1 Rectifier topologies . . . 31
2.2.3.2 Impedance matching network . . . 31
2.2.3.3 RF-to-DC conversion efficiency . . . 32
2.2.3.4 Schottky diode . . . 32
2.2.3.5 Effect of Schottky diode capacitance and resistance on the conversion efficiency . . . 33

2.2.3.6 Structure and operating principle of the rectifier . . . 33
2.2.3.7 DC filter . . . 34
2.2.3.8 Rectifier load . . . 34
2.3 Rectifier input impedance . . . 35
2.4 Power conversion efficiency . . . 35
2.5 Conclusion . . . 35

3 Design of a dual-band antenna for 2.45/5.8 GHz Wi-Fi applications 37
3.1 Introduction . . . 38
3.2 CST Studio microwave software . . . 38
3.3 Design process of proposed antenna . . . 38
3.3.1 Parametric study . . . 39
3.3.1.1 Reflection coefficient . . . 39
3.3.1.2 Radiation efficiency . . . 40
3.3.1.3 Realized gain . . . 41
3.3.2 Optimized design . . . 41
3.3.2.1 Reflection coefficient . . . 41
3.3.2.2 Radiation efficiency . . . 42
3.3.2.3 Realized gain . . . 43
3.3.3 Radiation Pattern . . . 43
3.3.4 Current distribution . . . 45
3.4 Conclusion . . . 46

4 A dual-band RF energy harvesting rectifier for 2.45/5.8 GHz Wi-Fi applications 47
4.1 Introduction . . . 48
4.2 Rectifier design . . . 48
4.3 Impedance matching on smith chart and reflection coefficient 49
4.4 DC output voltage response . . . 50
4.5 Power conversion efficiency (PCE) . . . 51
4.6 Performance comparison with the literature . . . 52
4.7 Conclusion . . . 52

General Conclusion 53

List of Figures

1.1 Wire antennas. 6
1.2 Aperture antennas. 7
1.3 Printed antennas. 8
1.4 Lens antennas 8
1.5 Input impedance of antenna. 10
1.6 The schematic equivalent of an antenna connected to a generator by a transmission line. 10
1.7 Estimation of the bandwidth of an antenna from its reflection coefficient curve. 12
1.8 Isotropical radiation pattern in vertical and horizontal planes. 14
1.9 Directional radiation pattern in the elevation plane. 15
1.10 Omnidirectional radiation pattern. 15
1.12 Cartesian representation of linear polarization. 17
1.13 Cartesian representation of circular polarization. 17
1.14 Cartesian representation of elliptical polarization. 18
1.15 Representation of radiation zones [7]. 19
1.16 Conventional patch antenna geometry [23]. 23
1.17 Representative shapes of micro-strip patch antenna. 24
1.18 coaxial probe feeding [23]. 25
1.19 Microstrip line feed patch antenna [23]. 25
1.20 Aperture coupled feed patch antenna [23]. 26
1.21 Proximity coupled micro-strip patch antenna [23]. 27

2.1 Energy harvesting principle. 30
2.2 Different configurations of the LC-matching networks 32
2.3 Equivalent circuit of the Schottky diode. 33
2.4 (a) Single diode (single stage); (b) Voltage doubler; (c) Voltage multiplier (multi-stage). 34
2.5 Voltage doubler rectifier. 35

3.1 Geometry of the proposed antenna. 39

3.2 Reflection coefficient magnitude of $|S_{11}|$ below −10 dB as a function of frequency for the 2.4 GHz and 5.8 GHz Wi-Fi bands of the proposed antenna. 40
3.3 Radiation efficiency of the proposed antenna for different values of the length P. 40
3.4 Realized gain in dBi as a function of frequency in GHz of the proposed antenna. 41
3.5 Reflection coefficient, $|S_{11}|$, in dB as a function of frequency in GHz of the proposed antenna. 42
3.6 Radiation efficiency of the proposed antenna. 42
3.7 Realized gain in dBi as a function of frequency in GHz of the proposed antenna. 43
3.8 3D radiation pattern at (a) 2.45 GHz and (b) 5.8 GHz. 44
3.9 Radiation patterns of the proposed antenna at 2.45 GHz and 5.8 GHz. 44
3.10 Surface current of the proposed antenna at 2.45 GHz and 5.8 GHz for $\omega t = 0°$ and $\omega t = 90°$. 45

4.1 Proposed rectifier schematic based on voltage-doubler rectifier. 49
4.2 Smith chart for impedance matching at (a) 2.45 GHz and (b) 5.8 GHz. 49
4.3 Reflection coefficient as a function of frequency for the proposed rectifier. 50
4.4 DC output voltage against frequency for the proposed rectifier. 51
4.5 Power conversion efficiency of the dual-band rectifier for 2.45/5.8 GHz 51

List of Tables

3.1 Dimensions of the proposed antenna. 39

4.1 Comparison with literature 52

List of Acronyms and Abbreviations

SWR	Standing Wave Ratio
RCF	Radiation Characteristic Function
HPBW	Half-power Beam-width
FBW	Fractional Bandwidth
RHEP	Right Handed Elliptical Polarization
LHEP	Left Handed Elliptical Polarization
AR	Axial ratio
GPS	Global Positioning System
DTV	Digital Television
GSM	Global System for Mobile Communications
MPA	Micro-strip Patch Antenna
CST	Computer Simulation Technology
EM	Electromagnetic
DC	Direct Current
AC	Alternative Current
Rectenna	Antenna and rectifier
ERP	Effective Radiated Power
ERIP	Equivalent Iso-tropically Radiated Power
ETSI	European Telecommunication Standards Institute
FCC	Federal Communication Commission
RF-EH	Radio Frequency Energy Harvesting
PCE	Power conversion efficiency
ADS	Advanced Design System
Wi-Fi	Wireless Fidelity
RF	Radio Frequency
VSWR	Voltage Standing Wave Ratio

List of Symbols

f_c	Central frequency
f_1	Lower frequency
f_2	Higher frequency
Z_C	Characteristic impedance
Z_{Ant}	Antenna impedance
R_{Ant}	Antenna resistance
X_{Ant}	Antenna reactance
R_{loss}	Loss resistance
$\Gamma(x)$	The reflection coefficient on a line
s_{11}	The reflection coefficient at the entrance to the antenna
ε	Dielectric permittivity
μ_r	Relative Permeability
h	Substrate Thickness
ε_r	Relative dielectric permittivity
$\tan\delta$	loss tangent
Δ f	Bandwidth
η	Radiation efficiency
$F(\theta,\varphi)$	Radiation characteristic function
$P(\theta,\varphi)$	Power in the direction(θ,φ)
$P(\theta_0,\varphi_0)$	Power in direction of maximum radiation
$D(\theta,\varphi)$	Directionality in direction (θ,φ)
$G(\theta,\varphi)$	Gain in direction (θ,φ)
P_t	Input power
P_r	Power at reception
G_t	Gain the transmitting antenna
G_r	Gain of receiving antenna
E	The electric field vector
E_x	The component of the electric field vector in the x direction
E_y	The component of the electric field vector in the y direction

H_x	The component of the magnetic field vector in the x direction
H_y	The component of the magnetic field vector in the y direction
f	The frequency in Hertz
ω	The pulsation in radians per second, equal to $2\pi f$
k	The wave number in radians per meter
φ_x	The initial phase of the E_x component
φ_y	The initial phase of the E_y component
τ	Transmission coefficient
G_t	Gain of the transmitting antenna
G_r	Gain of the receiving antenna
G	Gain
D	Directivity
Z_D	Total diode impedance
L_P	Parasitic inductance
R_S	Series resistance
R_j	Junction resistance
C_j	Junction capacitance
C_P	Parasitic capacitance
R_L	Load resistance
Z_{rec}	Total input impedance
P_{DC}	DC output power
P_{RF}	RFinput power
V_L	DC output voltage
R_{rad}	Antenna radiation resistance
λ	Wavelength

General Introduction

Radio Frequency Energy Harvesting (RFEH) is a crucial technique that converts electromagnetic (EM) energy into electrical energy in the form of a DC voltage. This technology is particularly attractive for body area networks, as it enables the wireless powering of low-energy sensors and electronic systems across various application environments through the extraction of energy from ambient RF sources [1]. Rectifiers are employed to convert alternating current (AC) voltage into direct current (DC) for powering various electronic devices, such as remote controls, RFID tags, Internet of things, and biotelemetry systems [2]. Depending on the application requirements, some devices demand high current levels, others require high voltages, while certain systems necessitate both high current and high voltage simultaneously [3].

Within the context of wireless power supply system development, we review some of the literature works. For example, authors Salhane et al. in [4], have designed an integrated electromagnetic rectification system (rectenna) using micro-strip technology on an FR4 substrate with optimized HSMS-2860 and HSMS-286C Schottky diode configurations. The antenna operates at 5.8 GHz, where a maximum power conversion efficiency (PCE) of 42.56% has been achieved by applying an input power of 20 dBm. The simulation results confirmed the system effectiveness for powering low-energy IoT devices and remote wireless sensors. Authors Prashad et al. in [5], have presented a dual-band electromagnetic energy harvesting rectenna for low-power applications, operating at 2.4 GHz and 5 GHz. The design employs a rectangular patch antenna enhanced with parasitic ground-plane stubs, integrated with a single-stage Greinacher voltage multiplier and a compact dual-band π-model matching network on an FR4 substrate. The results showed that the rectenna has achieved a peak power conversion efficiencies (PCE) of 68% at 2.4 GHz and 62% at 5 GHz. In a recent work in [6], a high-performance dual-band rectifier for radiofrequency energy harvesting (RF-EH) has been developed for the ISM bands at 2.45 GHz and 5.8 GHz. The proposed design utilized a series-configured SMS7621-005LF Schottky diode on a low-loss Rogers RT/duroid 5880 substrate, along with a hybrid dual-band impedance matching network based on quarter-wavelength transmission lines and open stubs. This is to improve the power transfer and suppress high order harmonics. Both simulation and experimental results have demonstrated peak power conversion efficiencies (PCE) of 34% at 2.45 GHz and 15% at 5.8 GHz at an input power of 10 dBm, demonstrating low PCE of the design.

Despite the promising prospects offered by the literature, the RFEH still

faces a major obstacle characterized by the decline in PCE, which is attributed to low input power levels. Accordingly, the core research issue is in designing rectifiers with improved PCE and ensuring their stability across the targeted frequency bands.

This work focuses on the design and simulation of a dual-band RF/ microwave energy harvesting rectenna for Wi-Fi applications together with a systematic evaluation of its performance. The proposed rectenna provides a high power conversion efficiency (PCE) compared to the literature. To clearly present the proposed approach and findings the manuscript is organized into four interconnected chapters.

Chapter one presents General Context of antennas. This chapter provides a comprehensive theoretical study of antennas and their classifications (wire aperture, printed, and optics-based). It details both the electrical parameters of antennas, such as impedance, reflection coefficient, and bandwidth. Also, their radiation parameters are presented, including radiation pattern, directivity, gain, and Friis transmission equation. Special emphasis is placed on patch antennas in terms of their design and constituent materials, concluding with an overview of their various feeding techniques, such as coaxial probe and microstrip line feeds.

Chapter two presents RF and Microwave energy harvesting systems. This chapter provides a comprehensive theoretical study of RF energy harvesting, reviewing its various ambient sources (such as Wi-Fi, mobile base stations/GSM, and DTV). It thoroughly analyzes the rectifier circuit, including rectifier topologies, impedance matching networks, and RF-to-DC power conversion efficiency. Furthermore, it details the characteristics of the Schottky diode—investigating the effects of its capacitance and resistance on conversion efficiency alongside the operating principles of the rectifier structure, DC filter, rectifier load, and input impedance.

Chapter three shows the design of the antenna part, which presents a dual-band antenna for 2.45/5.8 GHz Wi-Fi Applications. It presents the first practical phase of the research, conducted using CST Studio microwave software. It details the design process of the proposed antenna. Also, this section analyzes the simulated results for both stages, including the reflection coefficient, radiation efficiency, and realized gain, alongside investigating the radiation pattern and surface current distribution.

Chapter four demonstrates the second part, which is the rectifier. This latter is a dual-band RF energy harvesting rectifier designed for 2.45/5.8 GHz Wi-Fi Applications. The section focuses on the engineering and simulation of the rectifier stage. It describes the design process, highlighting

impedance matching implemented via the Smith chart and reflection coefficient analysis. Furthermore, it presents and discusses the performance results, specifically the DC output voltage, response, and power conversion efficiency (PCE), concluding with a performance comparison with existing literature to validate the effectiveness of the proposed design.

The manuscript ends with a general conclusion, highlighting the key outcomes of the work, which emphasize the main contributions and potential applications of the proposed rectenna.

Chapter 1

General context of antennas

Sommaire

1.1 Introduction 6

1.2 Antennas classification 6

1.2.1 Wire antennas 6

1.2.2 Aperture antennas 7

1.2.3 Printed antennas 7

1.2.4 Optics based antennas 8

1.3 Antenna parameters 8

1.3.1 Electrical parameters 9

1.3.2 Radiation parameters 13

1.4 Patch antenna 22

1.4.1 Overall 22

1.4.2 Basic patch antenna design 22

1.4.3 Dielectric materials 23

1.4.4 Conductive materials 24

1.5 Feeding techniques for patch antennas 24

1.5.1 Coaxial probe feeding 24

1.5.2 Micro-strip line feed 25

1.6 Conclusion 27

1.1 Introduction

Antennas are key elements of wireless communication systems because they allow electromagnetic waves to be transmitted and received through free space [7]. Their performance directly affects the efficiency and reliability of communication and energy-harvesting applications, making antenna theory an important field of study. This chapter presents the fundamental concepts of antenna theory, including antenna classifications, electrical and radiation characteristics, patch antennas, dielectric and conductive materials, and common feeding techniques [8]. These concepts provide the theoretical foundation required for the design and analysis of the proposed antenna discussed in the following chapter.

1.2 Antennas classification

Antennas are designed in a wide variety of shapes and designs. Although some antennas may not be easily classified, the majority can generally be organized into four primary categories: wire antennas, aperture antennas, printed-circuit antennas, and optical antennas. These main categories can be further classified into resonant antennas, broadband antennas, and electrically small antennas [9].

1.2.1 Wire antennas

The dipole and loop antennas are among the most common examples of classical wire antennas (see Figure 1.1).

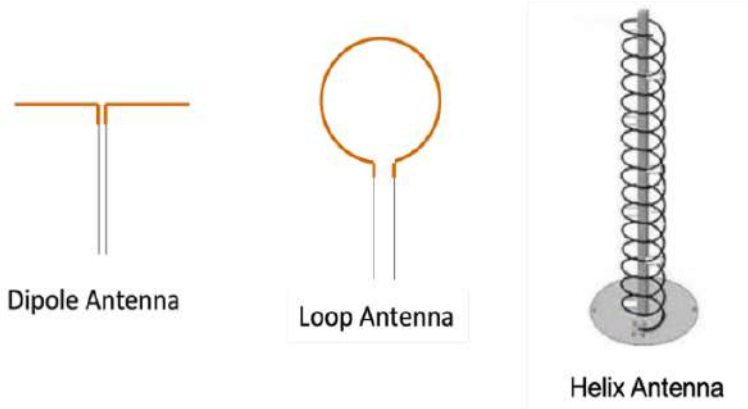

Figure 1.1: Wire antennas.

Their operation is based on the excitation of current at the feed point, which subsequently propagates along the wire structure and leads to the

radiation of electromagnetic waves. The overall length of the wire antenna is generally defined with respect to the wavelength corresponding to its operating frequency, which enables its classification as either electrically small or resonant. In most cases, dipole and loop antennas provide relatively low gain values, typically around 5 dBi or below. However, certain specialized wire antenna configurations, such as the helical antenna, can generate circular polarization, support wide bandwidths approaching an octave, and achieve higher gain levels ranging approximately from 8 to 15 dBi. [9]

1.2.2 Aperture antennas

A different class of antennas is known as aperture antennas (see Figure 1.2).

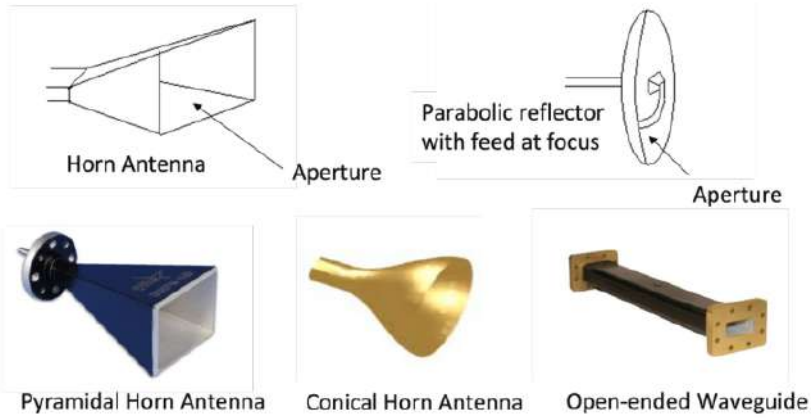

Figure 1.2: Aperture antennas.

The gain of these antennas is determined primarily by the size of their effective aperture. For example, horn antennas commonly provide gains on the order of 12 dBi or higher, whereas parabolic reflector antennas are capable of achieving significantly larger gains, often exceeding 30 dBi [9].

1.2.3 Printed antennas

Printed antennas, also known as patch antennas (Figure 1.3) represent a widely used and practical class of antennas. They are generally fabricated in simple geometrical forms, such as rectangular or circular shapes, on a dielectric substrate, with a conductive ground plane positioned on the opposite side [9].

Their bandwidth typically varies from a few percent to nearly 15%, depending on factors such as the substrate thickness and the feeding tech-

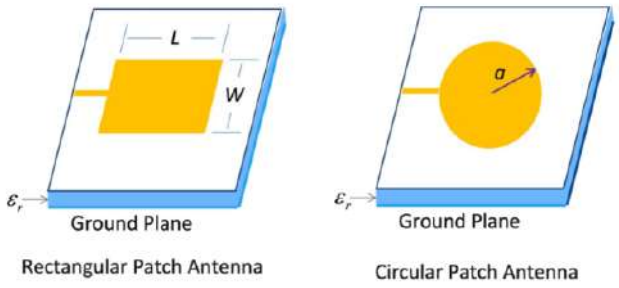

Figure 1.3: Printed antennas.

nique employed, including micro-strip, pin, or slot feeding methods. Due to their compact structure, they are extensively utilized in portable devices such as cell phones, where they are often designed in meandered-line configurations to accommodate space limitations [9].

1.2.4 Optics based antennas

Optics-based antennas, also referred to as lens antennas (Figure 1.4), are designed according to the principles of geometrical optics. This category includes structures such as lens antennas and parabolic antennas. In lens antennas, the feed is typically placed at the focal point, enabling the radiated wave to be transformed into an approximately plane wave as it propagates through the lens. Similarly, in parabolic dish antennas, a plane wave is generated through reflection from the curved reflecting surface, while secondary reflectors may be incorporated to enhance overall performance [9].

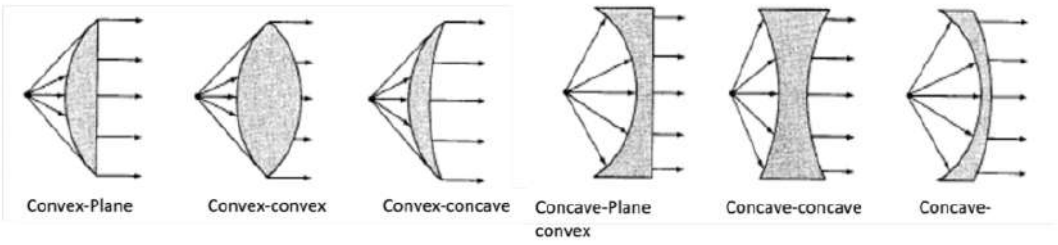

Figure 1.4: Lens antennas

1.3 Antenna parameters

The antenna is responsible for the conversion of electrical energy into electromagnetic energy, and vice versa. Energy is transferred from the transmitter to free space, where it propagates with the assistance of a transmit-

ting antenna. In contrast, a receiving antenna facilitates the reception of the energy of a wave propagating in space, thereby ensuring its transmission to a receiving device [10].

1.3.1 Electrical parameters

Electrical parameters characterize the antenna as an element of the connected circuit. They are used to evaluate the load presented by the antenna to the circuit and to determine the efficiency of power transfer between the antenna and the radio system. Thus, it can be concluded that the characteristics of an antenna can be classified into two distinct categories, namely electrical characteristics and radiation characteristics, based on the types of energy [10].

1.3.1.1 Input impedance

The input impedance of an antenna can be expressed as follows:

$$Z_{in} = R_{in} + jX_{in} = R_R + R_L + jX_{in} \tag{1.1}$$

where, R_{in}: denotes the resistive component of the antenna impedance R_R:represents the radiation resistance corresponding to the power radiated by the antenna, and R_L: refers to the loss resistance, which includes conduction losses, dielectric losses, and surface-wave losses. In addition X_{in}:corresponds to the reactive component of the antenna impedance, where:

$$X_{in} = L\omega - \frac{1}{C\omega}$$

Where ω denotes the angular frequency defined as ($\omega = 2\pi f$). Ideally, the radiation resistance R_R should be equal to zero and the input resistance R_{in} should match the impedance characteristics of the transmission line [10].

The imaginary part corresponds to the energy stored in the near-field region. If the matching conditions are not met, waves are reflected back toward the source, resulting in standing waves, measured by the Standing Wave Ratio (SWR). The amount of power an antenna radiates depends on the current flowing through it, with the highest radiation occurring at peak current. When the antenna is resonant, its impedance should be minimized to remain purely resistive. For optimal impedance matching ensuring maximum power transfer between the transmission line and the antenna the loss resistance R_P should be zero, and the radiation resistance R_r

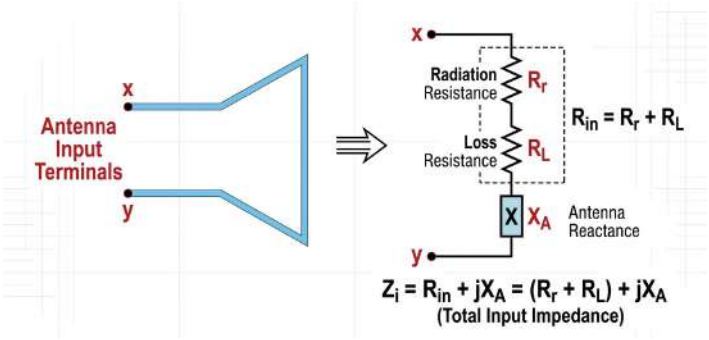

Figure 1.5: Input impedance of antenna.

should equal the transmission line's characteristic impedance [10].

The antenna efficiency can be expressed as follows:

$$\eta = \frac{R_{radiative}}{R_{radiative} + R_{loss}} \tag{1.2}$$

For improved antenna efficiency, the loss resistance should remain lower than the radiation resistance.

1.3.1.2 Reflection coefficient and the standing wave ratio

The reflection coefficient shows how much of an electromagnetic wave is reflected by an impedance discontinuity in the transmission medium. The reflection coefficient is equal to the ratio of the amplitude of the reflected wave (the wave returning to the generator) to the incident wave (the wave coming from the generator) [11].

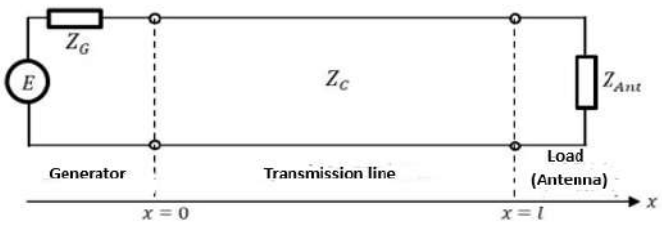

Figure 1.6: The schematic equivalent of an antenna connected to a generator by a transmission line.

$$\Gamma(x = l) = S_{11} = \frac{Z_{Ant} - Z_c}{Z_{Ant} + Z_c} \tag{1.3}$$

The transmission line is considered matched when $Z_{Ant} = Z_c$. Under this condition, the entire transmitted power is delivered to the load without any mismatch losses. The importance of impedance matching becomes evident when the impedances are not properly balanced, since a large portion of the incident power is then reflected back instead of being transferred to the load, which in this case is the antenna. The magnitude of the reflection coefficient S_{11} expressed in decibels (dB), is given by:

$$|S_{11}|_{(dB)} = 20\log|S_{11}| \tag{1.4}$$

The Voltage Standing Wave Ratio (VSWR) is a parameter used to evaluate the effectiveness of power transfer from the transmitter to the antenna system. It is defined as the ratio between the maximum voltage and the minimum voltage along the transmission line. The VSWR can be determined as follows:

$$\text{VSWR} = \frac{1+|S_{11}|}{1-|S_{11}|} \tag{1.5}$$

A significant impedance mismatch between the transmitter and the antenna, reflected by a high VSWR value, may lead to degraded transmission and reception performance [11].

1.3.1.3 Frequency bandwidth

The bandwidth or passband of an antenna is the frequency range in which the reflection coefficient remains below a specified threshold (Figure 1.7). It can also be described as the range of frequencies, where the energy transfer between the power source and the antenna (or from the antenna to the receiver) surpasses a defined limit, ensuring proper matching between the excitation source and the antenna.

An antenna bandwidth is typically determined from its reflection coefficient curve or, in some cases, its VSWR curve. It is generally defined by a reflection coefficient below -3 dB, -6 dB, -10 dB, or -15 dB, depending on the chosen criteria. However, the most widely used standard is the -10 dB threshold [12–14], which means that 90% of the energy from the source is successfully delivered to the antenna, and only 10% being reflected. The bandwidth is commonly viewed as a frequency range centered around the central frequency f_c, the bandwidth Δf is given by [10]:

$$\Delta f = f_2 - f_1 \tag{1.6}$$

Here f_1 and f_2 represent the lower and upper cutoff frequencies, respectively, defined at a specified threshold level. The relative fractional bandwidth (FBW) is expressed as a percentage and represents the ratio of the bandwidth to the center frequency fc which can be written as:

$$\text{FBW}(\%) = \frac{\Delta f}{f_c} \times 100 \tag{1.7}$$

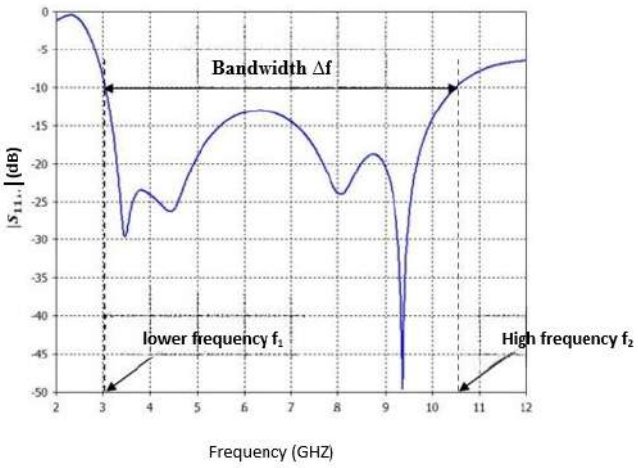

Figure 1.7: Estimation of the bandwidth of an antenna from its reflection coefficient curve.

1.3.1.4 Quality factor

The quality factor is an important characteristic of an antenna and is defined in a manner analogous to that used in linear electronic circuits. It is typically evaluated at the resonant frequency and is closely related to the antenna bandwidth. This parameter reflects the different loss mechanisms present in the antenna, including radiation losses, conduction losses, dielectric losses, and surface-wave losses. Consequently, the overall quality factor is influenced by all these loss components and can be expressed as [10, 15, 16]:

$$\frac{1}{\text{Q}_t} = \frac{1}{\text{Q}_{rad}} + \frac{1}{\text{Q}_c} + \frac{1}{\text{Q}_d} + \frac{1}{\text{Q}_{sw}} \tag{1.8}$$

where:
Q_t = total quality factor.

Q_{rad} = quality factor due to radiation(space wave) losses.
Q_c = quality factor due to conduction (ohmic) losses.
Q_d = quality factor due to dielectric losses.
Q_{sw} = quality factor due to surface waves.

1.3.2 Radiation parameters

The radiation parameters of an antenna describe its behavior in transmitting and receiving electromagnetic waves in space. Among these, the following characteristics are considered some of the most significant radiation properties of an antenna.

1.3.2.1 Radiation pattern

The antenna radiation pattern, also known simply as the antenna pattern, is a mathematical or graphical representation that describes the radiation characteristics of an antenna as a function of spatial coordinates. In most applications, these patterns are evaluated in the far-field region, where the angular distribution of the electromagnetic field becomes essentially independent of the distance from a reference point within the antenna region. The quantity represented by the radiation pattern is generally the normalized magnitude of the pattern function or one of its related parameters, such as directivity, partial directivity, gain, or partial gain. In some cases, other characteristics may also be represented, including the phase of a vector component of polarization-phase, the axial ratio, or the angle of tilt. These parameters are discussed in the following subsections [17].

1.3.2.2 Radiation characteristic function

The radiation characteristic function (RCF), denoted $F(\theta,\phi)$, is a graphical representation describing the ratio between the power radiated by an antenna in a given direction defined by the angles θ and ϕ, and the maximum radiated power $P(\theta_0,\phi_0)$ of the same antenna. In other words, the RCF corresponds to a normalized radiation pattern whose values range from 0 to 1 in linear scale (or down to 0 dB in logarithmic scale). This variation depends on the direction under consideration [10].

$$F(\theta,\phi) = \frac{P(\theta,\phi)}{P(\theta_0,\phi_0)} \tag{1.9}$$

Typically, radiation patterns are categorized into three primary types, which are:

- **Isotropic radiation**
  Isotropic radiation, as presented in Figure 1.8, refers to the uniform emission of electromagnetic energy in all directions with equal intensity, both horizontally and vertically. An isotropic antenna is therefore considered a theoretical radiating structure characterized by a gain of 1 (0 dB) throughout the entire spherical space surrounding it and an efficiency of 100%. Owing to these ideal properties, it is commonly employed as a reference antenna for evaluating antenna gain.

- **Directional radiation**
  An antenna that is capable of radiating or receiving electromagnetic waves more effectively in specific directions than in others is referred to as a directional antenna. This term is generally applied to antennas whose maximum directivity significantly exceeds that of a half-wave dipole. A typical directional radiation pattern is shown in Figure Figure 1.9.

- **Omnidirectional radiation**
  An omnidirectional antenna is characterized by its capability to radiate electromagnetic waves with uniform intensity in all directions within a given plane. A typical example of this type of antenna is the monopole antenna. Figure 1.10 presents a representative illustration of an omnidirectional radiation pattern.

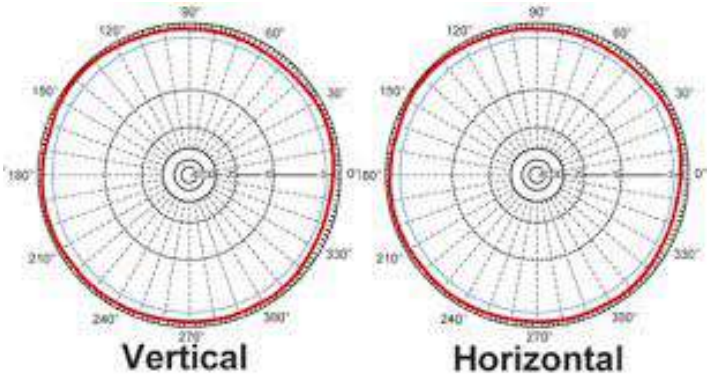

Figure 1.8: Isotropical radiation pattern in vertical and horizontal planes.

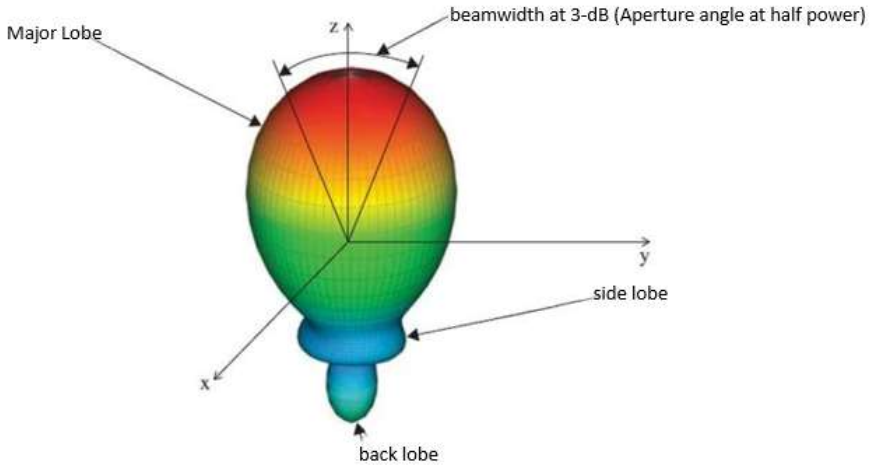

Figure 1.9: Directional radiation pattern in the elevation plane.

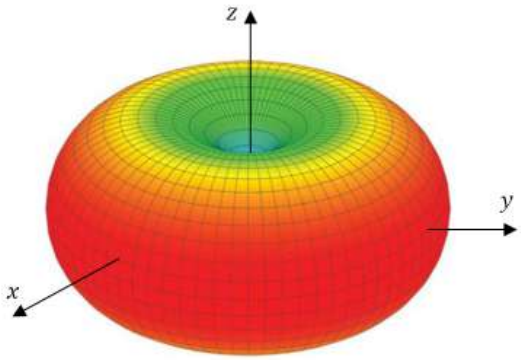

Figure 1.10: Omnidirectional radiation pattern.

1.3.2.3 Half-Power Beamwidth

The half-power beamwidth (HPBW) is defined, from a given cut of the radiation pattern, as the angular separation between the two directions at which the radiation intensity decreases to half of its maximum value. HPBW describes the antenna performance within the main lobe; however, it does not account for the amount of power radiated outside the principal beam. Consequently, additional parameters are generally employed to assess the directional characteristics of the antenna [17].

1.3.2.4 Field polarization

The polarization of an electromagnetic wave is defined by the trajectory traced over time by the electric field vector E or the magnetic field vector

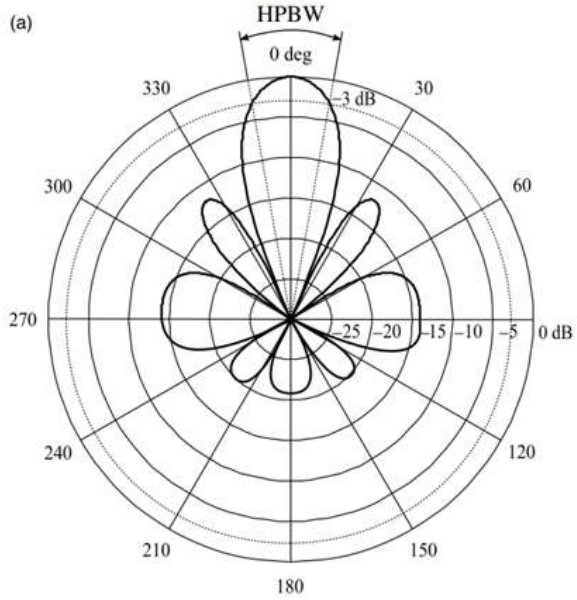

(a) The half-power beamwidth (HPBW).

H. Based on this behavior, three different types of polarization can be distinguished. Considering the z-axis as the direction of propagation, the field expression can be written as follows:

$$\mathrm{E}(z,t) = \hat{x}\mathrm{E}_x(z,t) + \hat{y}\mathrm{E}_y(z,t) \tag{1.10}$$

When the wave propagates along the positive z-direction, its trigonometric representation can be expressed as follows:

$$\mathrm{E}(z,t) = \hat{x}\mathrm{E}_{x_0}\cos(wt - kz + \varphi_x) + \hat{y}\mathrm{E}_{y_0}\cos(wt - kz + \varphi_y) \tag{1.11}$$

where E_{x_0} and E_{y_0} denote the amplitudes of the electric field components in the x- and y-directions, respectively; k represents the wave number; and φ_x and φ_y correspond to the initial phases of the two field components E_x and E_y, respectively. The three principal types of polarization are briefly presented below [10, 18, 19]:

a)Linear polarization

For a wave to exhibit linear polarization, the phase difference between the two field components must satisfy the following condition:

$$\Delta\varphi = \varphi_y - \varphi_x = n\pi, n = 0,1,2,3,... \tag{1.12}$$

Consequently, its trigonometric representation can be written as follows:

$$\mathrm{E}(z,t) = \hat{x}\mathrm{E}_{x_0}\cos(wt - kz) \pm \hat{y}\mathrm{E}_{y_0}\cos(wt - kz) \tag{1.13}$$

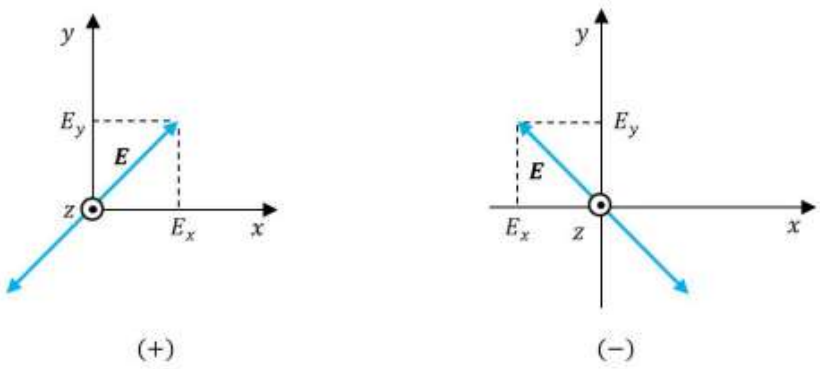

Figure 1.12: Cartesian representation of linear polarization.

Figure 1.12 illustrates the orientation of the electric field vector associated with linear polarization.

b)Circular Polarization

Circular polarization, as illustrated in Figure 1.13, occurs when the components of the electric field vector possess equal amplitudes and when the phase difference, $\Delta\varphi$, between the two components corresponds to an odd multiple of $\pi/2$. Thus,

$$\mathrm{E}_{x_0} = \mathrm{E}_{y0} \tag{1.14}$$

$$\Delta\varphi = \varphi_y - \varphi_x = n\pi = \begin{cases} +(\frac{1}{2}+2n)\pi, n = 1,2,\ldots & \text{for CW} \\ -(\frac{1}{2}+2n)\pi, n = 1,2,\ldots & \text{for CCW} \end{cases} \tag{1.15}$$

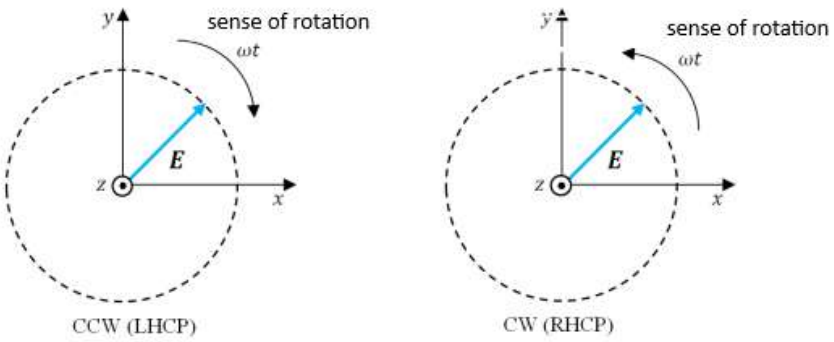

Figure 1.13: Cartesian representation of circular polarization.

c) Elliptical Polarization

For elliptical polarization, considering the particular case of an ellipse oriented along one of the principal axes, the amplitudes of the electric field

components are unequal. In addition, the phase difference between the two components corresponds to an odd multiple of $\pi/2$. Therefore,

$$E_{x_0} \neq E_{y0} \tag{1.16}$$

and

$$\Delta\varphi = \varphi_y - \varphi_x = n\pi = \begin{cases} +(\frac{1}{2}+2n)\pi, n = 1,2,... & \text{for CW} \\ -(\frac{1}{2}+2n)\pi, n = 1,2,... & \text{for CCW} \end{cases} \tag{1.17}$$

Figure 1.14 illustrates the ellipse described by the tip of the electric field vector as a function of time.

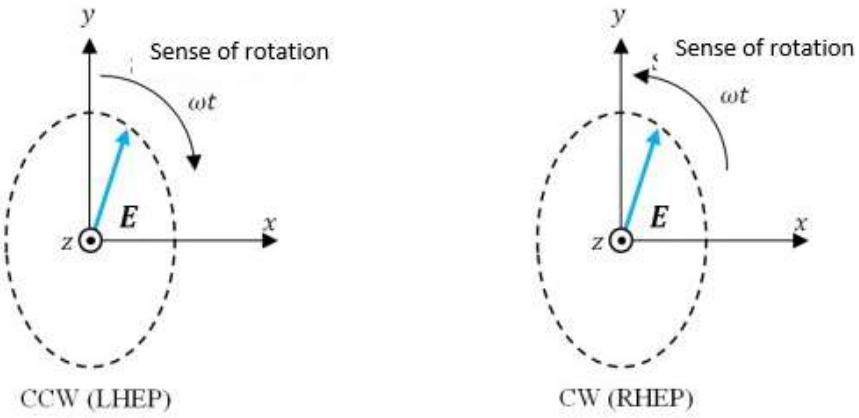

Figure 1.14: Cartesian representation of elliptical polarization.

The + and − signs in the equation correspond to left-hand elliptical polarization (LHEP) and right-hand elliptical polarization (RHEP), respectively. In Figure 1.14, the ellipse is generated by the trajectory traced over time by the tip of the electric field vector. The ratio between the semi-major axis and the semi-minor axis of the ellipse is referred to as the axial ratio, which satisfies the following relation: [10, 18–21]:

$$\text{AR} = \frac{\text{major axis}}{\text{minor axis}} \tag{1.18}$$

- When AR=1, the wave is circularly polarized .
- When AR approaches infinity, the wave exhibits linear polarization.

The axial ratio AR is generally expressed in decibels (dB).

$$\text{AR}_{d\text{B}} = 20\log_{10}(\text{AR}) \tag{1.19}$$

If the antenna exhibits an axial ratio below 3 dB, it is classified as circularly polarized.

1.3.2.5 Field regions

The space around an antenna is generally divided into three distinct regions: (a) the reactive near-field region, (b) the radiating near-field (Fresnel) region, and (c) the far-field (Fraunhofer) region, as illustrated in the figure 1.15.

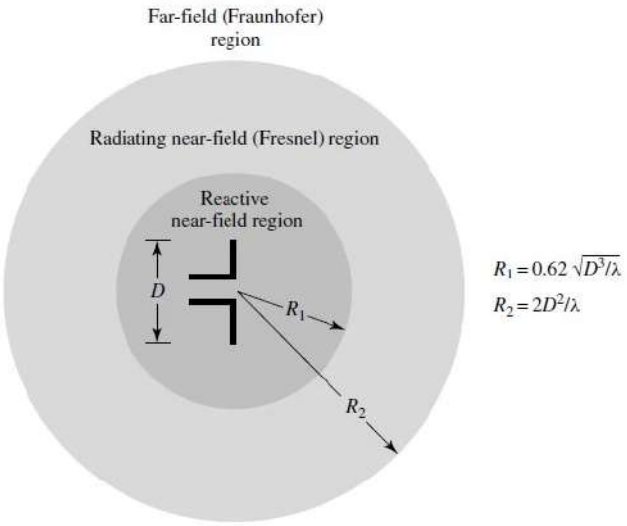

Figure 1.15: Representation of radiation zones [7].

a) Reactive near-field

The reactive near-field region refers to the space immediately surrounding the antenna, where the reactive field components are dominant. For most antennas, this region extends approximately up to $R < 0.62\sqrt{D^3/\lambda}$ from the antenna surface, where λ denotes the wavelength and D represents the largest dimension of the antenna. In the case of a very short dipole, this boundary is typically approximated as $\lambda/2\pi$, which is often considered the effective extent of the reactive near-field region.

b) Radiating near-field (Fresnel) region

The radiating near-field region is situated between the reactive near-field and the far-field regions of an antenna. In this zone, the radiated field components are predominant, and the angular field distribution still varies with the distance from the antenna. The Fresnel region is another term used to describe the radiating near-field, based on an optical analogy in which the radiation is considered to be focused at infinity. Considering D as the largest dimension of the antenna, the inner boundary of this

region is given by $R < 0.62\sqrt{D^3/\lambda}$, while the outer boundary is defined as $R < 2D^2/\lambda$. These limits are based on a maximum allowable phase error of $\pi/8$. In this region, the radial field component may still be significant, and the radiation pattern generally depends on the radial distance.

c) far-field region

The far-field region refers to the space surrounding an antenna where the angular field distribution becomes independent of the distance from the antenna. This region is generally assumed to start at distances greater than $2D^2/\lambda$. However, this criterion may not be fully applicable to certain antenna types, such as multi-beam reflector antennas, whose far-field behavior can be affected by phase variations across their apertures. In this region, the electromagnetic field components are predominantly transverse, and the radiation pattern remains unchanged with respect to radial distance. The lower limit of the far-field region is defined as $R = 2D^2/\lambda$, while its upper limit extends theoretically to infinity.

1.3.2.6 Antenna directivity

The directivity of an antenna in a specified direction is defined as the ratio of the power radiated in that direction to the power that would be radiated by an isotropic antenna.

More generally, it can be expressed as the ratio between the radiation intensity in a given direction and the radiation intensity of an isotropic source radiating the same total power.

$$D(\theta,\phi) = \frac{P(\theta,\phi)}{P_{iso}} = \frac{P(\theta,\phi)}{P_{rad}/4\pi} \tag{1.20}$$

If no direction is specified, the reference is taken as the direction of maximum radiation intensity, corresponding to the maximum directivity, which is given by:

$$D_{max} = D_0 = \frac{P_{max}}{P_{iso}} = \frac{4\pi P_{max}}{P_{rad}} \tag{1.21}$$

1.3.2.7 Antenna gain

The antenna gain differs from its directivity only by the efficiency η of the antenna:

$$G(\theta,\varphi) = \eta D(\theta,\varphi) \tag{1.22}$$

In general, the antenna gain refers to the gain in the direction of maximum radiation. This parameter describes the ability of the antenna to concentrate radiated power in a preferred direction. The gain is typically expressed in decibels (dB) as follows:

$$G_{(dB)} = 10\log_{10}(G) \tag{1.23}$$

The radiation intensity associated with the isotropically radiated power is obtained by dividing the power accepted by the antenna (input power) by 4π. In equation form, this can be expressed as:

$$G = 4\pi \frac{\text{radiation intensity}}{\text{total input (accepted) power}} = 4\pi \frac{P(\theta,\phi)}{P_{in}} \tag{1.24}$$

1.3.2.8 Radiation efficiency

The radiation efficiency η of an antenna quantifies the fraction of power lost between the RF source and the surrounding propagation medium. It is defined as the ratio of the total radiated power P_r to the input (accepted) power P_a supplied to the antenna [10].

$$\eta = \frac{P_r}{P_a} \tag{1.25}$$

The antenna gain is therefore related to its directivity in linear terms as follows:

$$G = \frac{P(\theta,\phi)}{P_a/4\pi} = \eta \frac{P(\theta,\phi)}{P_r/4\pi} = \eta D((\theta,\phi) \tag{1.26}$$

1.3.2.9 Friis Transmission Equation

A telecommunications system considering a transmitting antenna with gain G_t, fed by a power P_t, and a receiving antenna with gain G_r. The system is described as follows [10]:

$$p_r = \frac{P_t G_t}{4\pi d^2} \tag{1.27}$$

The power P_r received by an antenna with an equivalent effective area A_r, located at a distance d, is given by [10]:

$$P_r = p_r A_r, \text{where } A_r = \frac{G_r \lambda^2}{4\pi} \tag{1.28}$$

The Friis transmission equation, also known as the telecommunications formula, can therefore be expressed as follows:

$$P_r = P_t G_t G_r \left(\frac{\lambda}{4\pi d}\right)^2 \tag{1.29}$$

This leads to the Friis transmission equation, which defines the free-space path loss A_0 as follows:

$$A_0 = \frac{P_r}{P_t} = \left(\frac{\lambda}{4\pi d}\right)^2 G_t G_r \tag{1.30}$$

The first term in this expression is referred to as the propagation loss.

1.4 Patch antenna

1.4.1 Overall

Nowadays, micro-strip patch antennas, commonly referred to as patch antennas, are widely used across various applications worldwide [13]. This antenna type was initially developed in the 1970's. Its low-profile structure and lightweight nature, compared to parabolic reflectors and other antenna systems, made it particularly suitable for airborne and space applications. More recently, the use of high dielectric constant materials has enabled further miniaturization, which has contributed to the widespread adoption of patch antennas in mobile devices, GPS receivers, and other mass-produced wireless technologies.

1.4.2 Basic patch antenna design

Figure 1.16 presents the basic configuration of a conventional micro-strip patch antenna (MPA). The structure comprises a conducting radiating patch positioned on a dielectric substrate characterized by its relative permittivity (ε_r) and relative permeability (μ_r), while a conducting ground plane is placed on the opposite side of the substrate. The antenna is excited through a micro-strip feed line connected to a signal source, enabling the transfer of electromagnetic energy to the radiating element. The substrate thickness (h) and dielectric properties significantly influence the antenna's electrical characteristics, including resonant frequency, impedance bandwidth, radiation efficiency, and gain. Radiation is primarily generated by the fringing electric fields around the edges of the patch, which convert guided waves into free-space electromagnetic waves. Due to its compact

profile, low manufacturing cost, and ease of integration with microwave circuits and printed circuit technologies, the micro-strip patch antenna has become one of the most widely adopted antenna structures in contemporary wireless communication systems [7, 22].

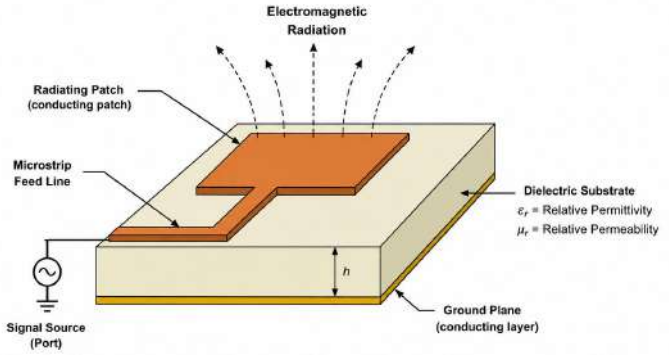

Figure 1.16: Conventional patch antenna geometry [23].

1.4.3 Dielectric materials

Dielectric materials are commonly employed as an intermediate layer between the radiating element and the ground surface [10]. A dielectric is mainly characterized by two fundamental parameters: the relative permittivity ε_r and the loss tangent $\tan\delta$ [23]. These parameters significantly influence the antenna performance and its overall characteristics. In order to be suitable for micro-strip applications, such materials should satisfy several requirements [10]:

- Adequate mechanical strength to support the overall structure.
- Sufficient thermal conductivity to avoid overheating issues.
- High hydro-phobic, since moisture degrades material performance.
- Very low dielectric losses.
- Minimal dispersion.
- Low anisotropy with nearly linear behavior.
- Uniform and homogeneous material composition.

1.4.4 Conductive materials

The conductive material section plays a crucial role in determining the performance of the patch antenna. Copper is the most commonly used material due to its high electrical conductivity, corrosion resistance, and ease of fabrication. Aluminum is also used as an alternative, although it is less frequently adopted than copper. Depending on the design requirements, other conductive materials with appropriate electrical and manufacturing properties may also be considered. The radiating patch can be implemented in various geometries, such as square, rectangular, thin strip (dipole), triangular, circular ring, elliptical, or combinations of these forms. Figure 1.17 illustrates several examples of these geometries. Although each shape exhibits specific characteristics, square, rectangular, and circular patches are the most commonly used due to their simplicity in fabrication and analysis [24].

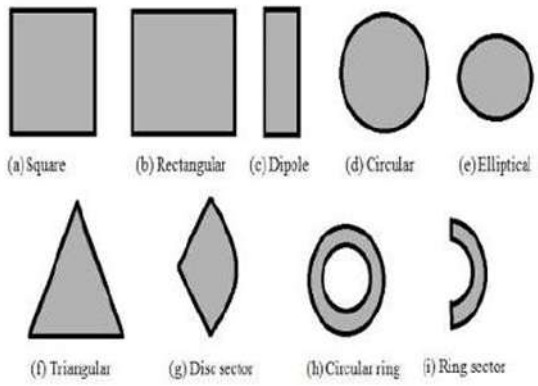

Figure 1.17: Representative shapes of micro-strip patch antenna.

1.5 Feeding techniques for patch antennas

A feeding is employed to excite the antenna and initiate radiation through either direct or indirect coupling. Various feeding techniques exist, among which the most commonly used are coaxial probe feeding, micro-strip line feeding, aperture coupling, and proximity coupling [23].

1.5.1 Coaxial probe feeding

Coaxial probe feeding is a technique in which the inner conductor of a coaxial cable is connected to the radiating patch of the antenna, while the outer conductor is linked to the ground plane. This feeding method offers

several advantages, including simple fabrication, easy impedance matching, and low spurious radiation. However, it also presents some drawbacks, such as limited bandwidth and increased modeling complexity, particularly when thick substrates are used. Figure 1.18 illustrates this configuration [23].

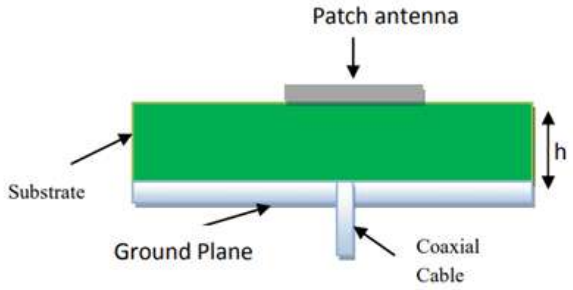

Figure 1.18: coaxial probe feeding [23].

1.5.2 Micro-strip line feed

Micro-strip line feeding is one of the simplest fabrication techniques, as it consists of a conducting strip directly connected to the radiating patch, effectively acting as an extension of it. This method is easy to model and allows straightforward impedance matching by adjusting the inset position. However, its main limitation is that increasing the substrate thickness leads to higher surface wave excitation and spurious feed radiation, which consequently restricts the achievable bandwidth [23].

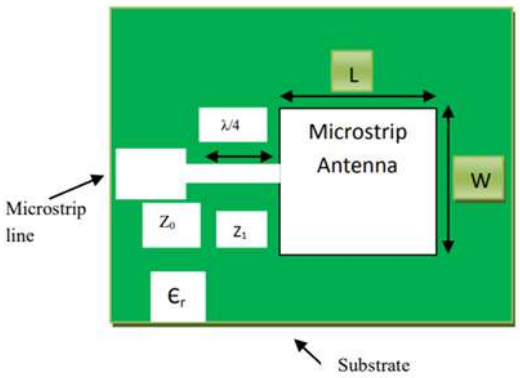

Figure 1.19: Microstrip line feed patch antenna [23].

1.5.2.1 Aperture coupled feed

Aperture-coupled feeding consists of two separate dielectric substrates that are divided by a common ground plane. On the lower substrate, a micro-

strip feed line is printed, and its energy is transferred to the radiating patch through a slot (aperture) etched in the ground plane. This configuration enables independent optimization of both the feeding network and the radiating element. Typically, the upper substrate is chosen to be relatively thick with a low dielectric constant, while the lower substrate has a higher dielectric constant. The central ground plane provides isolation between the feed line and the radiating patch, thereby reducing unwanted coupling and minimizing spurious radiation, which improves radiation pattern quality and polarization purity. The main advantage of this technique is the flexibility it offers in independently optimizing the feed structure and the radiating element [23].

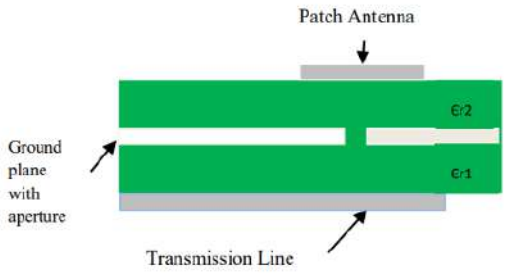

Figure 1.20: Aperture coupled feed patch antenna [23].

1.5.2.2 Proximity coupling

Proximity coupling provides the widest bandwidth and exhibits very low spurious radiation. However, its main limitation lies in the complexity of its fabrication process. Impedance matching is typically controlled by adjusting the length of the feeding stub and the width-to-length ratio of the radiating patch. The coupling mechanism in this feeding technique is primarily capacitive in nature [23].

The main drawback of this feeding technique is its fabrication complexity, as it requires precise alignment of two dielectric layers. In addition, this structure leads to an increase in the overall thickness of the antenna. Among the various configurations of micro-strip antennas, there are several geometries; however, in general, a micro-strip antenna is composed of four fundamental elements [23]:

They are:

- The radiating patch
- The dielectric substrate

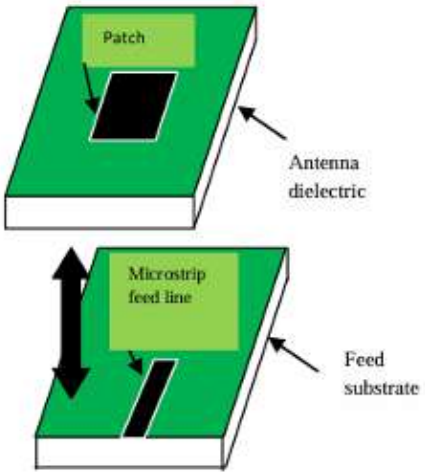

Figure 1.21: Proximity coupled micro-strip patch antenna [23].

- The ground plane
- The feed line

1.6 Conclusion

This chapter has presented the fundamental theoretical concepts related to antennas and their role in wireless communication systems. Various antenna classifications were reviewed, followed by a detailed discussion of the key electrical and radiation parameters that govern antenna performance, including impedance matching, reflection coefficient, bandwidth, radiation pattern, polarization, directivity , gain, and efficiency. The chapter also introduced micro-strip patch antennas, emphasizing their structure, material characteristics, and design requirements. In addition, the principal feeding techniques employed for patch antennas were examined. The theoretical knowledge established throughout this chapter provides a solid basis for understanding and evaluating the antenna proposed in this work and serves as a foundation for the design and simulation procedures presented in the subsequent chapter.

Chapter 2

RF and microwave energy harvesting systems

Sommaire

2.1 Introduction 29

2.2 RF Energy Harvesting 29

2.2.1 Description 29

2.2.2 RF energy sources 30

2.2.3 Rectifier circuit 31

2.3 Rectifier input impedance 35

2.4 Power conversion efficiency 35

2.5 Conclusion 35

2.1 Introduction

To date, radio frequency (RF) energy harvesters have demonstrated distinct advantages over alternative ambient energy sources, such as solar, acoustic, and mechanical vibration systems. The primary merits of RF energy harvesting (RF-EH) technology namely its reliability, predictability, controllability, and the capacity for simultaneous power delivery to multiple distributed nodes—render it a preferred solution for specialized applications and environments [1][2]. Although the volume of harvested energy remains relatively modest, this technology is highly effective for low-power applications deployed across extensive, decentralized node networks [3]. Generally, RF energy sources are classified into ambient and intentional categories [3]. Intentional RF energy relies on dedicated sources designed to transmit targeted signals to specific areas [4]. Recent advancements in semiconductor technology and fabrication processes have played a pivotal role in the practical realization of these harvesting systems. By converting electromagnetic (EM) waves into usable electrical power, RF-EH facilitates the continuous operation of low-power sensors [5]. Conversely, ambient RF energy is ubiquitously available across a diverse spectrum of frequency bands. These include Long-Term Evolution (LTE: 750–800 MHz), Digital Television (DTV: 550–600 MHz), Universal Mobile Telecommunications System (UMTS: 2150–2200 MHz), GSM-900 (850–910 MHz), GSM-1800 (1850–1900 MHz), and Wi-Fi (2.4–2.45 GHz). Additionally, it spans conventional television and radio broadcasting bands (900 MHz–2 GHz), as well as Industrial, Scientific, and Medical (ISM: 2.1–2.6 GHz), UltraWideband (UWB: 3.1–10.6 GHz), Wireless Local Area Network (WLAN: 3.1–4.4 GHz), High Performance Radio Local Area Network (HIPERLAN: 5.1–5.3 GHz), and C-band (4.4–5 GHz) spectra [6] [25].

2.2 RF Energy Harvesting

2.2.1 Description

Radio Frequency Energy Harvesting (RFEH) is increasingly recognized as a promising solution for sustainably powering small, connected devices, particularly within the Internet of Things (IoT) ecosystem [1–5] [26]. The concept is simple yet impactful: the surrounding environment is filled with unseen radio waves generated by mobile networks, Wi-Fi routers, broadcast stations,and numerous communication systems [1]. Rather than al-

lowing this energy to dissipate, RFEH systems capture these signals, convert them into electrical power, and utilize it to operate devices such as wireless sensor nodes (WSNs), often eliminating the need for conventional batteries [3],[5] [25]. An RFEH-based wireless system typically works through four main stages[2],[4],as shown in Figure. 2.1.

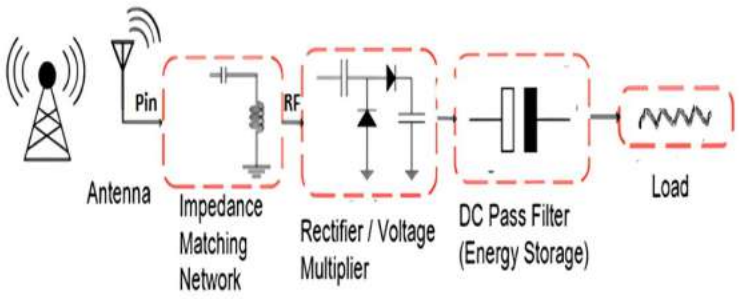

Figure 2.1: Energy harvesting principle.

2.2.2 RF energy sources

This section highlights the main RF enrgy sources, include Wi-Fi, GSM/ cellular, and TV/DTV as the primary sources for RF energy harvesting. Figure 10 illustrates the RF power densities of these sources measured outside the Northfields London Underground station [17], showing that GSM 900/1800 bands provide the highest power levels. Although other sources, such as AM radio stations and UHF RFID, have potential, their availability remains limited [27].

2.2.2.1 Energy harvesting from wi-Fi sources

Between 2012 and 2016, research on Wi-Fi energy harvesting showed steady progress. Early studies powered low-energy devices and sensors, followed by improvements in rectifier efficiency and communication capabilities. By 2015, wi-Fi systems could power sensors cameras and charge batteries using Wi-Fi signals [27].

2.2.2.2 Mobile bases station/GSM/cellular sources

Over the past two decades, mobile communication has expanded rapidly, with over 7.3 billion users worldwide. This growth has led to an increase in cellular base stations which, along with mobile phones, generate RF signals for communication. In GSM systems, the main operating frequencies are 900 MHz and 1800 MHz. Among these, the 900 MHz band is widely

used for RF energy harvesting due to its lower propagation loss and better long-distance transmission compared to higher-frequency bands like 3G and Wi-Fi (2.4 GHz) [27].

2.2.2.3 TV and DTV sources

Early studies demonstrated the potential of harvesting RF energy from TV and DTV signals. In 2009, Intel Research harvested 60 μW at a distance of 4 km from a TV tower. Later, Mikeka et al. developed a rectenna with efficiencies of 18.2 and 0.4 at different input levels. In 2013, Parks et al. powered a wireless sensor using DTV signals from 10.4 km away. Since TV signals are continuously broadcast and largely unaffected by weather, they offer a reliable and sustainable source for ambient energy harvesting [27].

2.2.3 Rectifier circuit

2.2.3.1 Rectifier topologies

The microwave rectifier can adopt various topologies depending on how the diodes are arranged for rectification. Among these, series and shunt configurations are the most commonly discussed in the literature. Additionally, to enhance the output DC voltage, voltage doubler or voltage multiplier topologies can also be employed [28].

2.2.3.2 Impedance matching network

When a rectifier circuit is not properly matched to the receiving antenna, part of the incoming power is reflected instead of being absorbed, reducing the power available for rectification. Therefore, an impedance matching network is essential to ensure proper matching between the antenna and the circuit. Common matching networks include L, π, and T configurations. The choice depends on the design goal: an L-network is suitable for single-band matching, while π and T networks are preferred when additional functions like harmonic rejection or band-pass filtering are required.

The π-network also offers a wider bandwidth than the L-network. Matching circuits can use lumped elements (capacitors and inductors) or distributed elements (such as stubs and microstrip lines). At high frequencies, distributed elements are favored because lumped components suffer from parasitic effects. In microstrip technology, an open-circuit stub be-

haves like a parallel capacitor, while a short-circuit stub acts as a parallel inductor [29].

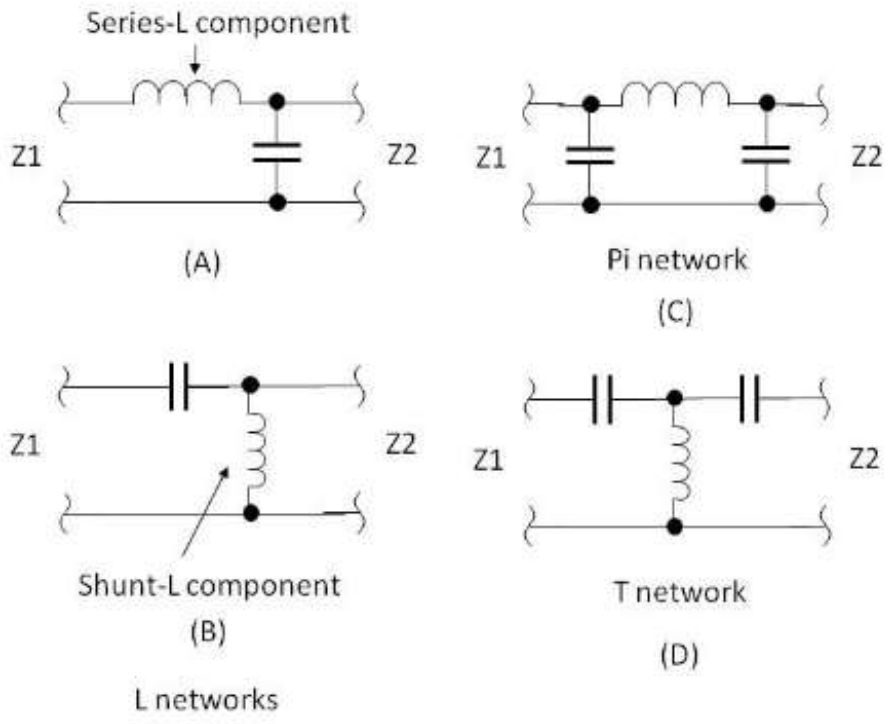

Figure 2.2: Different configurations of the LC-matching networks

2.2.3.3 RF-to-DC conversion efficiency

A Schottky diode circuit connected to an antenna is used for RF-to-DC power conversion. To maximize the conversion of incident RF power into DC, the rectifier must achieve high efficiency. This depends on the type of Schottky diode, the ability to suppress harmonics, proper load resistance selection, and the capability to handle arbitrarily polarized incident waves [30].

2.2.3.4 Schottky diode

Conventional PN junction diodes, typically used at low frequencies, have high junction capacitance, making them unsuitable for high-frequency applications. In contrast, Schottky diodes use a metal semiconductor junction, resulting in much lower capacitance and better performance at high frequencies, such as RF-to-DC rectification. The effects of junction capacitance and resistance will be discussed in the next section [30].

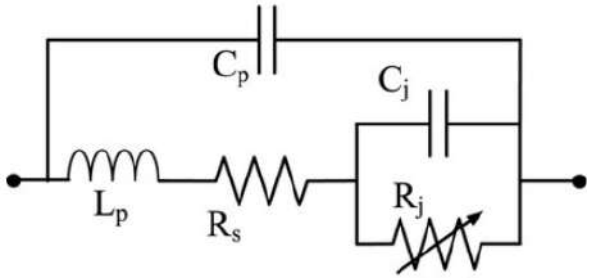

Figure 2.3: Equivalent circuit of the Schottky diode.

The impedance of the Schottky diode, according to its ECM in Figure 2.3, is given by,

$$Z_D = jL_p\omega + \frac{\left(R_s + \frac{R_j}{1+jR_jC_j\omega}\right) \times \frac{1}{jC_p\omega}}{\left(R_s + \frac{R_j}{1+jR_jC_j\omega}\right) + \frac{1}{jC_p\omega}} \tag{2.1}$$

2.2.3.5 Effect of Schottky diode capacitance and resistance on the conversion efficiency

According to [4], the junction capacitance (C_j) shifts the tuned frequency and causes mismatch, so a low value (around 0.2 pF) is recommended, especially at high frequencies. For the junction resistance R_j, smaller values improve matching at 2 GHz, while higher values (10 kΩ) cause mismatch without shifting the frequency. Another method for improving high-frequency rectenna efficiency is discussed in [30].

2.2.3.6 Structure and operating principle of the rectifier

A rectifier is an electronic circuit designed to convert alternating current (AC) into direct current (DC) to power a load. In the field of RF energy harvesting, diode rectifiers also known as uncontrolled rectifiers, are the most commonly used devices due to their simplicity and fast response. Generally, these rectifying circuits can be classified into different topologies depending on the required output voltage and application requirements [31]. As illustrated in 2.4, these configurations include:

(a) A single-diode rectifier (single-stage): This topology uses a single diode in series with a load to eliminate the negative half-waves of the signal whilst leaving the positive half-waves intact, operating as a basic half-wave rectifier.

(b) A voltage doubler: This configuration utilizes diodes and storage capacitors to effectively double the peak amplitude of the input AC voltage at the output load.

(c) A multi-stage voltage multiplier: This circuit converts low input AC voltages into higher positive DC voltages by cascading multiple rectifying stages and switching between the conducting diodes during the positive and negative half-waves thereby ensuring efficient voltage boosting and power conversion .

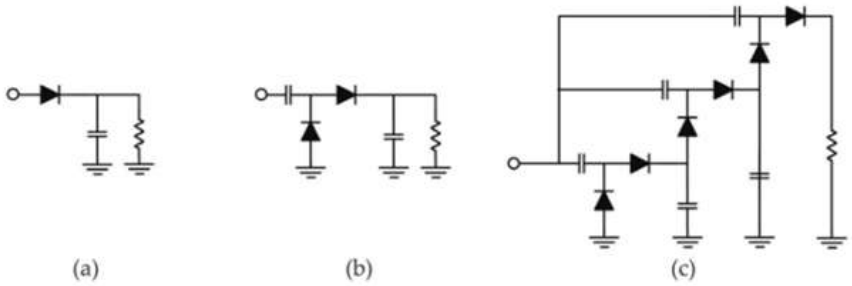

Figure 2.4: (a) Single diode (single stage); (b) Voltage doubler; (c) Voltage multiplier (multi-stage).

2.2.3.7 DC filter

The DC filter is a low-pass filter, usually made of a capacitor placed in parallel with the load. It blocks the fundamental signal and its harmonics after the diode. Its cutoff frequency must be lower than the fundamental frequency, and the capacitor value is calculated by using the equation as follows [28],

$$C = \frac{1}{2\pi f_c} \tag{2.2}$$

2.2.3.8 Rectifier load

The load is defined as a component or a network of electrical elements (either passive or active) connected to the output of the rectifier circuit. Its primary function is to consume the rectified Direct Current (DC) power extracted from ambient Radio Frequency (RF) signals.

Devices encompass a broad spectrum of energy-consuming components and sensors. This category primarily includes Internet of Things (IoT) modules, biomedical implants, environmental monitoring systems and low-power communication units [32].

2.3 Rectifier input impedance

The choice of the appropriate network circuit depends on requirements such as higher output or wider bandwidth, but the efficiency of the corresponding network changes as the output impedance changes. In combine harvesters, the load is the input impedance of the rectifier [33]. To compute the rectifier input impedance of the circuit in Figure 2.5, we use the following expression [2],

$$Z_{rec} = \frac{1}{jC_1\omega} + Z_D // \left\{ Z_D + \left(\frac{1}{jC_2\omega} // R_L \right) \right\} \tag{2.3}$$

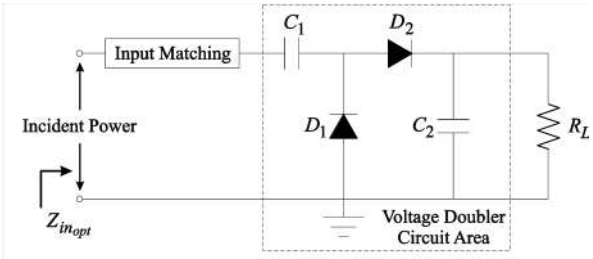

Figure 2.5: Voltage doubler rectifier.

2.4 Power conversion efficiency

The key parameters to be optimized when designing a rectifier circuit are the DC output voltage and the RF-to-DC power conversion efficiency (PCE). The latter represents the ratio between the DC power obtained at the rectifier output (P_{DC}) and the RF power supplied at its input (P_{RF}) from a microwave source. This efficiency is calculated using equation 2.4 [2].

$$PCE(\%) = \frac{P_{DC}}{P_{RF}} \times 100\% = \frac{V_L^2}{R_L P_{RF}} \times 100\% \tag{2.4}$$

where P_{DC} is the DC power delivered to the load R_L; P_{RF} is the input power at the rectifier input; and V_L is the DC output voltage [28].

2.5 Conclusion

In conclusion, energy harvesting represents a transformative approach toward self sustaining electronic systems. This chapter has demonstrated that, while various ambient sources exist, RF energy harvesting stands out due to wireless signals. We have concluded that the overall efficiency of

such systems is strictly dictated by the performance of the rectenna and the precision of the impedance matching circuit. These theoretical insights are crucial as we look to design a specialized antenna capable of effectively capturing low-density ambient energy.

Chapter 3

Design of a dual-band antenna for 2.45/5.8 GHz Wi-Fi applications

Sommaire

3.1 Introduction 38
3.2 CST Studio microwave software 38
3.3 Design process of proposed antenna 38
3.3.1 Parametric study 39
3.3.2 Optimized design 41
3.3.3 Radiation Pattern 43
3.3.4 Current distribution 45
3.4 Conclusion 46

3.1 Introduction

In this chapter, we present the design and simulation of a dual-band antenna for Wi-Fi use. This antenna operates at 2.45 GHz and 5.8 GHz. All results of the proposed antenna are obtained using CST Studio microwave software. We start with a parametric study, showing the mean parameters that affect antenna performance. Then, we show the final results of the optimized antenna in terms of reflection coefficient, gain, radiation efficiency, radiation pattern, and surface current, which demonstrate high performance for 2.45/5.8 GHz dual-band Wi-Fi applications.

3.2 CST Studio microwave software

Computer simulation technology (CST) studio is a 3-D simulator software used for designing and analyzing electromagnetic systems. It is widely used in designing RF and microwave devices, include antennas, filters, splitters, power dividers, couplers, etc. It supports both time and frequency domain analysis, computing scattering parameters and field distributions. It is used in industry and academia to reduce prototyping costs and shorten development time. It is known for its high accuracy and user-friendly graphical interface for design and simulation.

3.3 Design process of proposed antenna

The design of the proposed antenna, presented in Figure 3.1, consists of two monoples with different lengths to cover two bands of Wi-Fi applications. The design is implemented on a Rogers AD 430 substrate, with a relative permittivity of $\varepsilon_r = 4.3$ and a loss tangent of $tan\delta = 0.003$. The overall dimensions of the proposed antenna are $35 \times 38 \times 1.6\ mm^3$. First, a 50 Ω microstrip feed line with a width $W_f = 3$ mm and a length F = 28 mm is designed to ensure proper impedance matching. Next, the feed line is connected to a meandered monopole structure defined by the parameters S = 7.5 mm, d = 6 mm, and P = 5.5 mm. This folded structure increases the electrical current path within a compact size, allowing the antenna to resonate at the lower 2.45 GHz Wi-Fi band. Finally, a partial ground plane with a length L_g = 18 mm is introduced on the bottom layer to enhance the impedance bandwidth. In addition, a secondary vertical stub characterized by C = 11 mm, B = 3 mm, and A = 6 mm generates the second

resonance required for the upper 5.8 GHz Wi-Fi band. Therefore, the proposed antenna geometry provides a good compromise between compact size, impedance matching, and dual-band radiation performance, making it suitable for ambient RF energy harvesting systems.

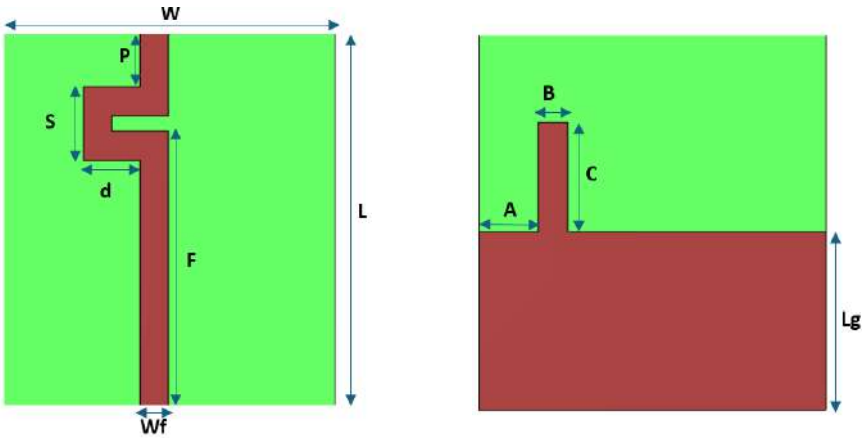

(a) Top view. (b) Bottom view.

Figure 3.1: Geometry of the proposed antenna.

Table 3.1: Dimensions of the proposed antenna.

Parameter	L	W	F	Lg	C	S	A	d	P	B	Wf	h
Value (mm)	38	35	28	18	11	7.5	6	6	5.5	3	3	1.6

3.3.1 Parametric study

3.3.1.1 Reflection coefficient

Figure 3.2 presents the parametric study of the reflection coefficient magnitude $|S_{11}|$ of the proposed antenna for different values of the parameter P (P = 5.5 mm, 9.5 mm, and 13.5 mm). The obtained results show that the variation of P strongly influences the resonant frequency and the impedance matching performance of the antenna. For P = 5.5 mm, the resonance is observed at higher frequencies, whereas increasing P to 9.5 mm and 13.5 mm shifts the resonance toward lower frequencies. This behavior confirms the inverse relationship between the antenna length and the resonant frequency, where an increase in the effective antenna length leads to a decrease in the operating frequency according to the relations $L = \lambda/2$ and $f = c/\lambda$. Moreover, the proposed antenna achieves $|S_{11}| < -10$ dB within the targeted 2.4 GHz and 5.8 GHz Wi-Fi bands, indicating good impedance matching and efficient antenna operation.

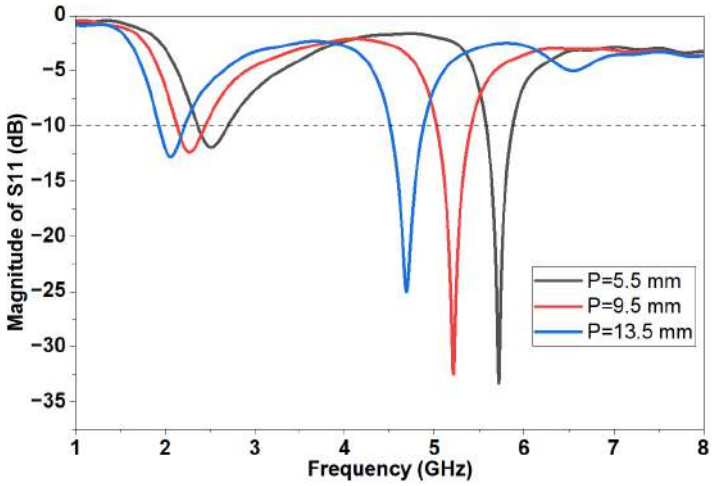

Figure 3.2: Reflection coefficient magnitude of $|S_{11}|$ below −10 dB as a function of frequency for the 2.4 GHz and 5.8 GHz Wi-Fi bands of the proposed antenna.

3.3.1.2 Radiation efficiency

Figure 3.3 presents a parametric study of the radiation efficiency of the proposed antenna for different values of the parameter P values of 5.5 mm, 9.5 mm, and 13.5 mm as a function of frequency.

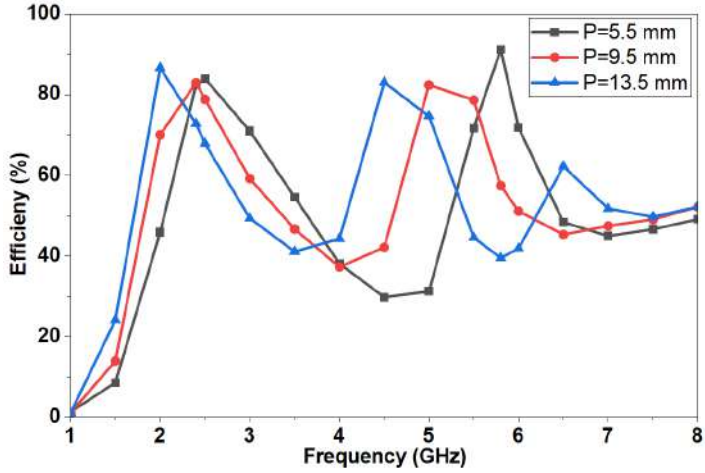

Figure 3.3: Radiation efficiency of the proposed antenna for different values of the length P.

The results show that the variation of P has a clear impact on radiation efficiency and overall antenna performance. It can be observed that the antenna performs well in the operating frequency bands, especially around 2.4 GHz and 5.8 GHz. For P = 5.5 mm and P = 9.5 mm, the efficiency remains above 50% over a wide frequency range, with peak values close to 90%, while for P = 13.5 mm it still maintains acceptable performance around these bands. In general, a radiation efficiency above 50% is considered satisfactory, as it indicates efficient radiation with reduced losses. Therefore, the obtained results confirm that the proposed antenna

exhibits stable radiation performance for all studied values of P, making it suitable for operation in the 2.4 GHz and 5.8 GHz bands.

3.3.1.3 Realized gain

Figure 3.4 shows the parametric study of the realized gain as a function of frequency for different values of the length P. The results indicate that varying P affects the gain response and the position of the gain peaks.

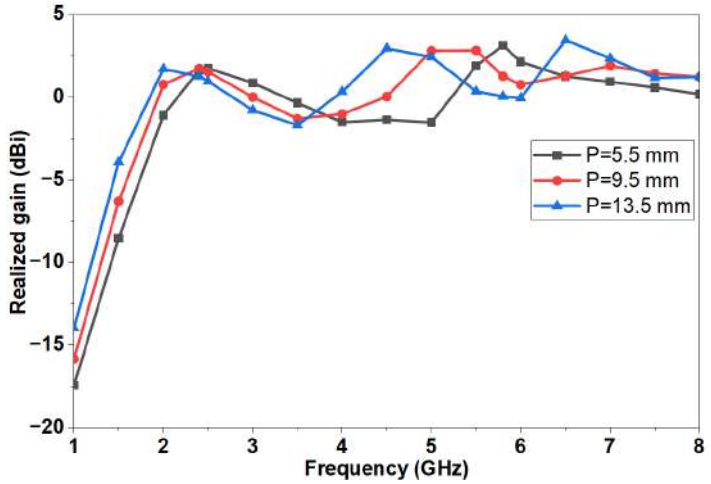

Figure 3.4: Realized gain in dBi as a function of frequency in GHz of the proposed antenna.

The realized gain remains positive within the operating bands, demonstrating efficient radiation performance. Therefore, the parameter P plays an important role in optimizing the antenna performance at the desired resonant frequencies.

3.3.2 Optimized design

3.3.2.1 Reflection coefficient

Figure 3.5 presents the magnitude of the reflection coefficient, $|S_{11}|$ in dB, as a function of frequency in GHz for the proposed antenna. The results demonstrate a clear dual-band operation satisfying the standard impedance matching criterion of $|S_{11}| \leq -10$ dB, which ensures that over 90% of the incident power is successfully transmitted to the antenna structure. The first operating band is centered around 2.45 GHz with a minimum $|S_{11}|$ of approximately −12 dB and a −10 dB fractional bandwidth spanning from 2.3477 GHz to 2.7223 GHz.

The second band exhibits a much deeper resonance at 5.7294 GHz, reaching a minimum $|S_{11}|$ of −33.33 dB with an impedance bandwidth from 5.5756 GHz to 5.8736 GHz. This pronounced negative peak at the higher

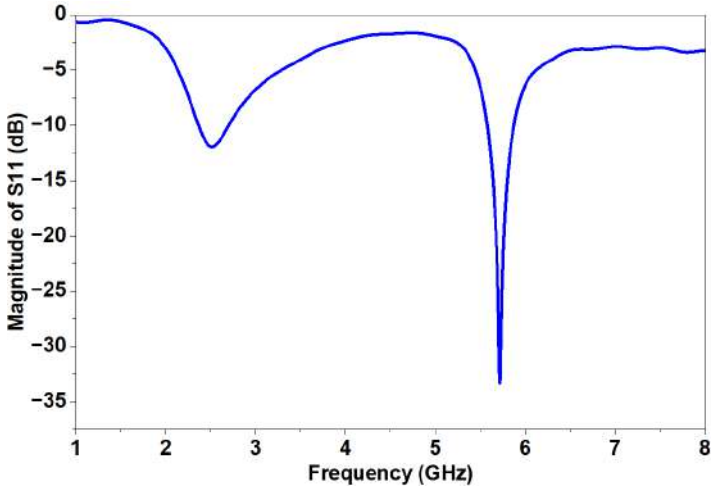

Figure 3.5: Reflection coefficient, $|S_{11}|$, in dB as a function of frequency in GHz of the proposed antenna.

band signifies near-perfect impedance matching with negligible reflection losses, thereby optimizing the antenna's overall power transfer efficiency.

3.3.2.2 Radiation efficiency

Figure 3.6 presents the radiation efficiency of the 2.4/5.8 GHz antenna versus frequency variation. High radiation efficiencies of 83.23% at 2.45 GHz and 91.16% at 5.8 GHz are obtained.

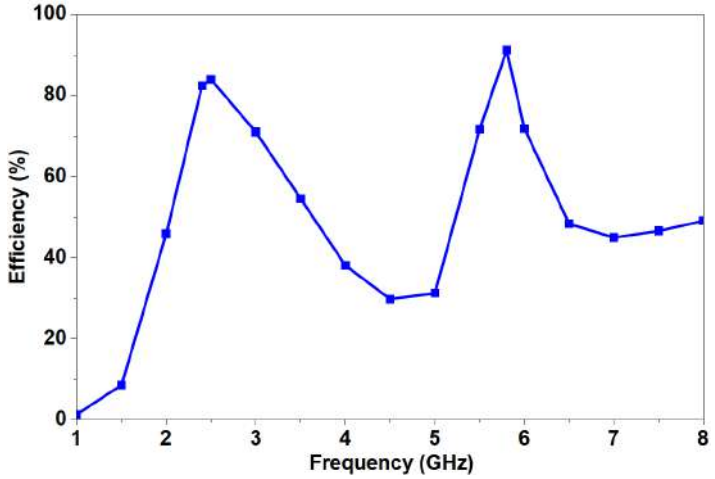

Figure 3.6: Radiation efficiency of the proposed antenna.

These high values demonstrate that most of the accepted power is effectively radiated, while only a small portion is lost due to conductor and dielectric losses. Therefore, the proposed antenna exhibits excellent radiation characteristics and reliable overall performance. Generally, an antenna with a radiation efficiency greater than 50% is considered to have good performance.

3.3.2.3 Realized gain

Figure 3.7 shows the realized gain in dBi as a function of frequency in GHz for the proposed antenna. The obtained results indicate peak realized gains of 1.75 dBi at 2.45 GHz and 3.15 dBi at 5.8 GHz. These positive gain values demonstrate the ability of the antenna to radiate electromagnetic energy efficiently with suitable directivity over the targeted Wi-Fi frequency bands. In addition, the stable gain response ensures reliable signal transmission and reception, which enhances the overall performance of the antenna for wireless communication applications.

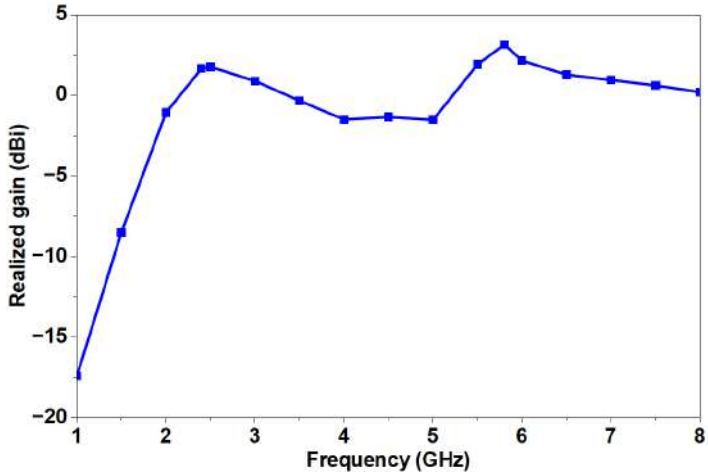

Figure 3.7: Realized gain in dBi as a function of frequency in GHz of the proposed antenna.

3.3.3 Radiation Pattern

The proposed antenna shows directional radiation at 2.45 GHz and 5.8 GHz, as shown in Figure 3.8. The color scale indicates the radiation intensity, where red corresponds to the maximum radiation gain and blue represents the minimum radiation levels. The antenna achieves a peak gain of approximately 1.88 dBi at 2.45 GHz, which increases to about 2.15 dBi at 5.8 GHz. In both frequency bands, the radiation pattern remains stable and well-defined, with a slightly higher directivity observed at 5.8 GHz. These results demonstrate the ability of the proposed antenna to provide effective radiation performance for dual-band wireless communication applications.

Figure 3.9 shows the radiation patterns of the proposed antenna at 2.45 GHz and 5.8 GHz for $\varphi = 0°$ and $\varphi = 90°$. The antenna exhibits a bidirectional radiation pattern at both frequencies, radiating most of its energy in two opposite directions. At 2.45 GHz, the pattern is smooth and stable, with a

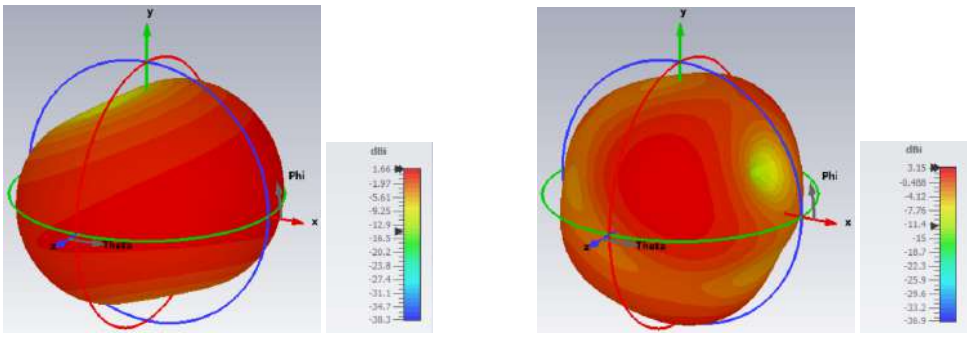

(a) (b)

Figure 3.8: 3D radiation pattern at (a) 2.45 GHz and (b) 5.8 GHz.

maximum gain of about 1.73 dBi. At 5.8 GHz, the pattern becomes slightly different in shape, but the bidirectional behavior is maintained. The gain increases to approximately 5.9 dBi, indicating better radiation performance at the higher frequency. These results demonstrate that the proposed antenna provides suitable radiation characteristics for dual-band Wi-Fi applications.

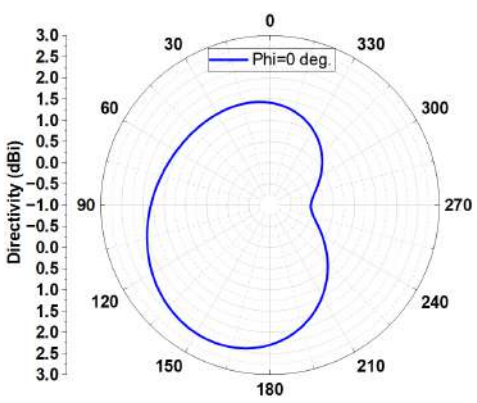

(a) φ = 0° at 2.45 GHz.

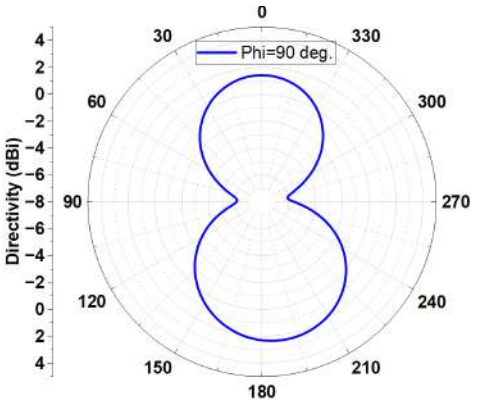

(b) φ = 90° at 2.45 GHz.

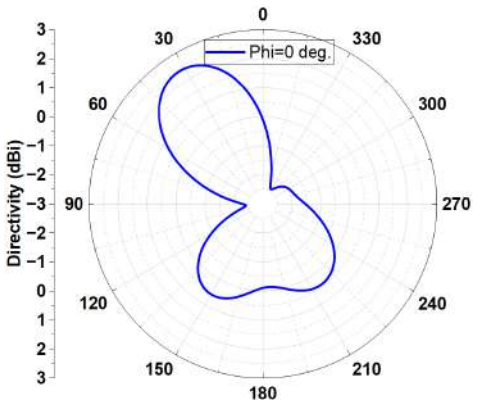

(c) φ = 0° at 5.8 GHz.

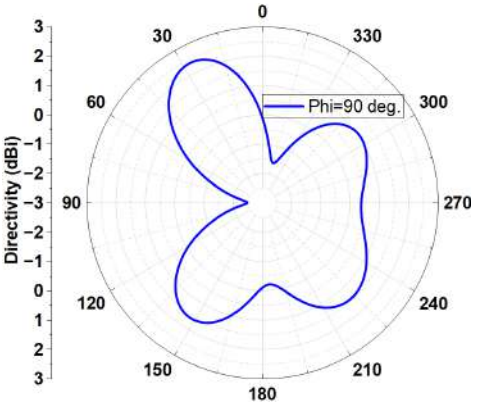

(d) φ = 90° at 5.8 GHz.

Figure 3.9: Radiation patterns of the proposed antenna at 2.45 GHz and 5.8 GHz.

3.3.4 Current distribution

Figure 3.10 shows the surface current distribution of the proposed antenna at 2.45 GHz and 5.8 GHz for phase angles of $\omega t = 0°$ and 90°. At 2.45 GHz, the current is mainly concentrated along the central meandered strip, indicating that this section is responsible for the lower-frequency resonance. At 5.8 GHz, the current is more concentrated around the side stub and the upper part of the ground plane, showing their contribution to the higher-frequency resonance. The different current paths at the two frequencies confirm that separate parts of the antenna generate each operating band, allowing the antenna to achieve efficient dual-band performance.

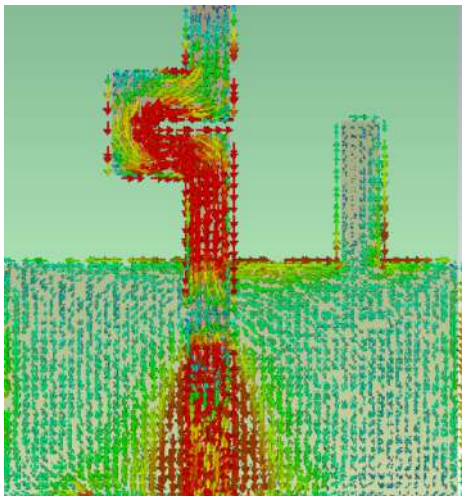

(a) $\omega t = 0°$ at 2.45 GHz.

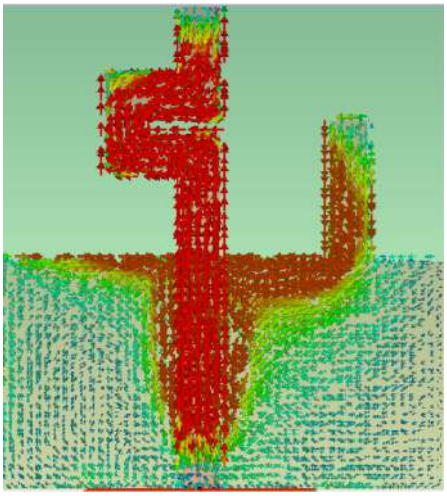

(b) $\omega t = 90°$ at 2.45 GHz.

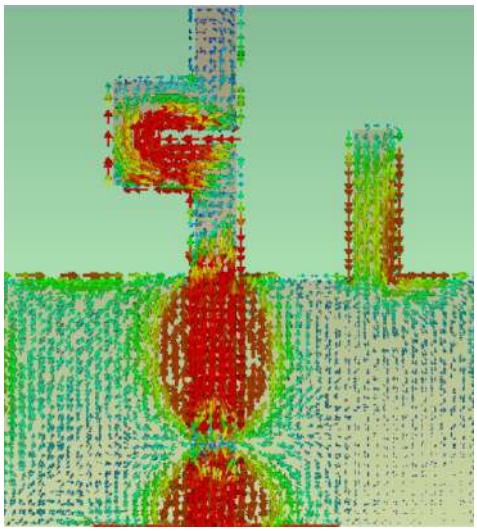

(c) $\omega t = 0°$ at 5.8 GHz.

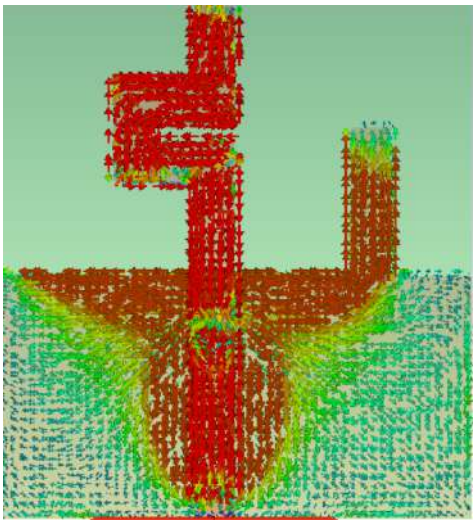

(d) $\omega t = 90°$ at 5.8 GHz.

Figure 3.10: Surface current of the proposed antenna at 2.45 GHz and 5.8 GHz for $\omega t = 0°$ and $\omega t = 90°$.

3.4 Conclusion

In this chapter, we have designed a dual-band antenna for Wi-Fi applications, covering 2.45 GHz and 5.8 GHz. The proposed design has demonstrated excellent performance over the operating frequency bands. High peak values of realized gain of 1.73 dBi and 5.9 dBi have been, respectively, obtained at 2.45 GHz and 5.8 GHz, with radiation efficiencies of 83.23% and 91.16%. With the performance achieved, the antenna shows high suitability for dual-band Wi-Fi energy harvesting applications.

Chapter 4

A dual-band RF energy harvesting rectifier for 2.45/5.8 GHz Wi-Fi applications

Sommaire

4.1 Introduction 48
4.2 Rectifier design 48
4.3 Impedance matching on smith chart and reflection coefficient 49
4.4 DC output voltage response 50
4.5 Power conversion efficiency (PCE) 51
4.6 Performance comparison with the literature 52
4.7 Conclusion 52

4.1 Introduction

This chapter focuses on the practical aspect, namely the design and performance analysis of the system key component: the rectifier. The main objective here is to design a dual-band rectifier characterized by high efficiency at the most common bands in Wi-Fi applications. This chapter covers the design methodology, starting with the selection of suitable diodes and extending to the construction of a matching network using the Smith Chart. The results of simulations carried out using ADS software are also be presented, with a focus on key performance metrics such as the reflection coefficient (S_{11}), DC output voltage (V_L), and power conversion efficiency (PCE). The chapter ends with concluding remarks and perspectives.

4.2 Rectifier design

The proposed rectifier is presented in Figure 4.1. The latter is designed to convert the radio-frequency (RF) signals received from the antenna into a stable DC voltage, making it suitable for low-power 2.45/5.8 GHz Wi-Fi applications. To ensure maximum power transfer, impedance matching is achieved using L-section networks. For the 2.45 GHz path, an L-section comprising a series capacitor of C = 0.416 pF and a parallel inductor of L = 3.96 nH, which matches the 50 Ω source impedance to the rectifier impedance of $Z_{in} = 49.46 - j0.23\ \Omega$. Similarly, for the 5.8 GHz path, also an L-section with a series capacitor of C=0.213 pF and a parallel inductor of L=0.637 nH is utilized to match the source to a rectifier impedance of $Z_{in} = 50.21 + j0.18\ \Omega$ at the latter frequency.

Each path employs a pair of SMS7630 Schottky diodes, specifically selected for their low threshold voltage to enhance rectification efficiency. Furthermore, each path is terminated with a capacitive low-pass filter to suppress residual high-frequency harmonics. Finally, the outputs from both tracks are combined to deliver power to a common load resistance $R_L = 2.7\ k\Omega$.

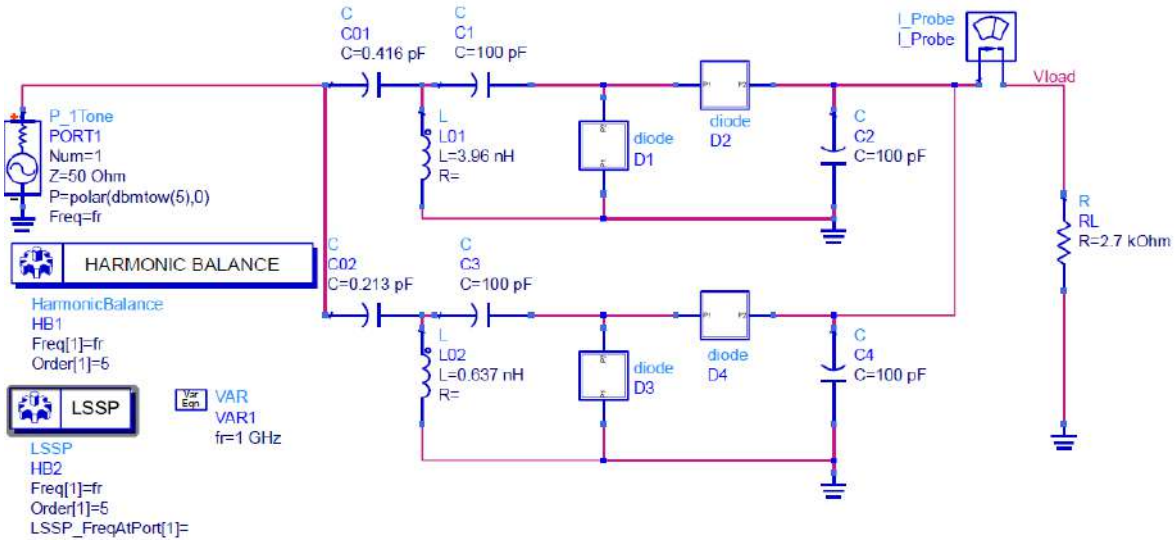

Figure 4.1: Proposed rectifier schematic based on voltage-doubler rectifier.

4.3 Impedance matching on smith chart and reflection coefficient

In order to match the rectifier input impedance to the antenna impedance, we have used the Smith Chart respectively at 2.45 GHz (Fig. 4.2a) and 5.8 GHz (Fig. 4.2b).

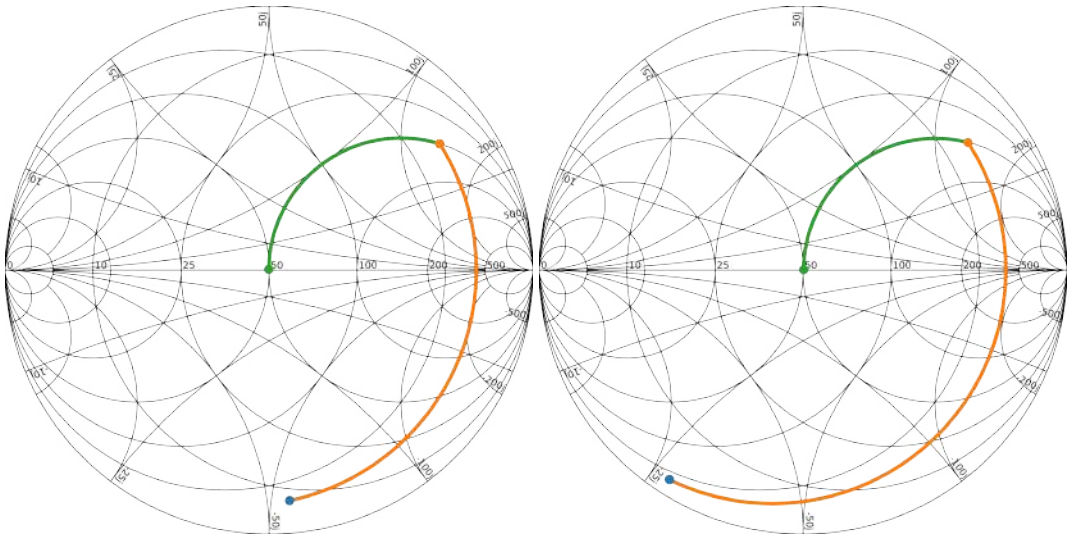

(a) 2.45 GHz (b) 5.8 GHz

Figure 4.2: Smith chart for impedance matching at (a) 2.45 GHz and (b) 5.8 GHz.

To achieve optimal impedance matching, a Smith chart was employed to design the required L-section networks for both operating frequencies. For the 2.45 GHz path the network incorporates a series capacitor C = 0.416 pF and a parallel inductor L = 3.96 nH to match the 50 Ω source impedance with the rectifier input impedance of $Z_{in} = 49 - j0.23$ Ω, likewise for the

5.8 GHz path an L-section consisting of a series capacitor C = 0.213 pF and a parallel inductor L = 0.637 nH is utilized to match the source to an impedance of $Z_{in} = 50.21 + j0.18\ \Omega$.

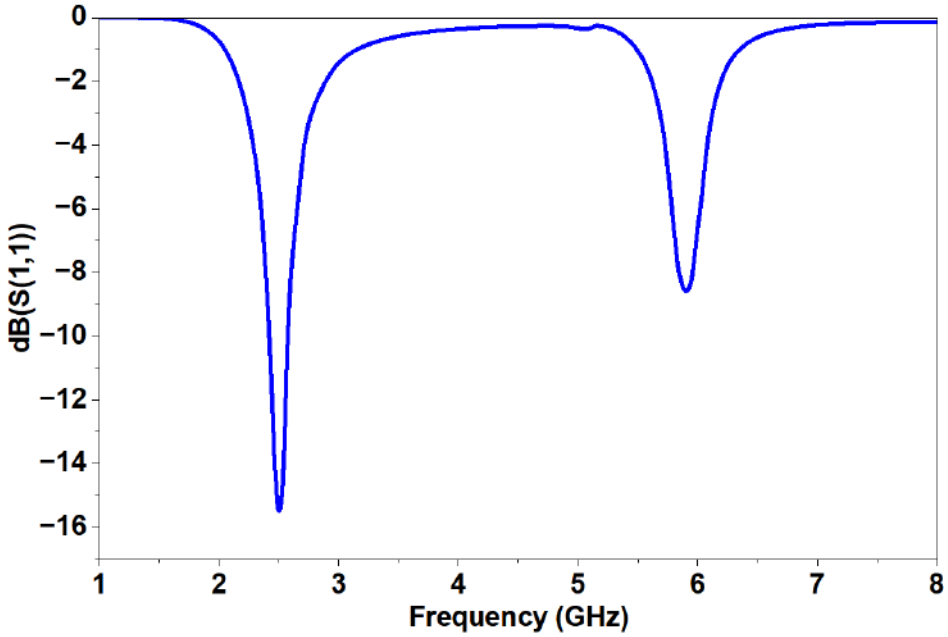

Figure 4.3: Reflection coefficient as a function of frequency for the proposed rectifier.

Figure 4.3 displays the reflected power level at the rectifier input as a function of frequency. The dual-band rectifier achieves low reflection coefficients of -15.5 dB at 2.45 GHz and -8.6 dB at 5.8 GHz, as highlighted in the plot. The -15.5 dB value indicates excellent impedance matching at the lower band, while the -8.6 dB at the upper band still represents a very good match, confirming a well-optimized interface between the antenna and the rectifier circuit with minimal reflection losses over both operating frequencies.

4.4 DC output voltage response

The measured DC output voltage is recorded as a function of frequency. Figure 4.4 demonstrates that, at the first resonant frequency of 2.45 GHz, the DC output voltage reaches a peak value of 2.43 V. Similarly, at the second resonant frequency of 5.8 GHz, the DC output voltage is recorded at 2 V. These results signify a high AC-to-DC conversion efficiency confirming the rectifier's effectiveness in harvesting electromagnetic energy across Wi-Fi bands.

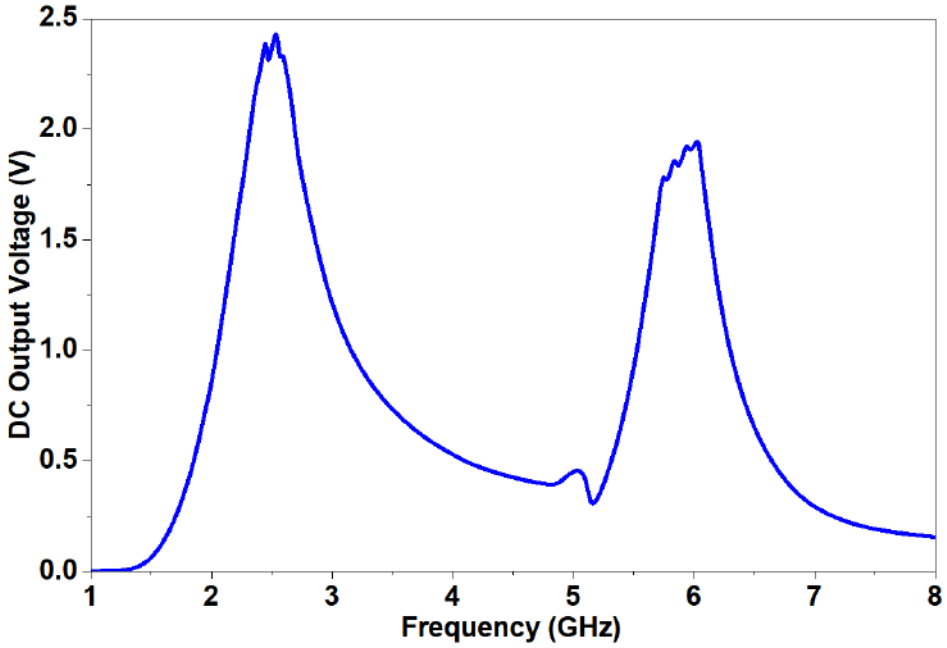

Figure 4.4: DC output voltage against frequency for the proposed rectifier.

4.5 Power conversion efficiency (PCE)

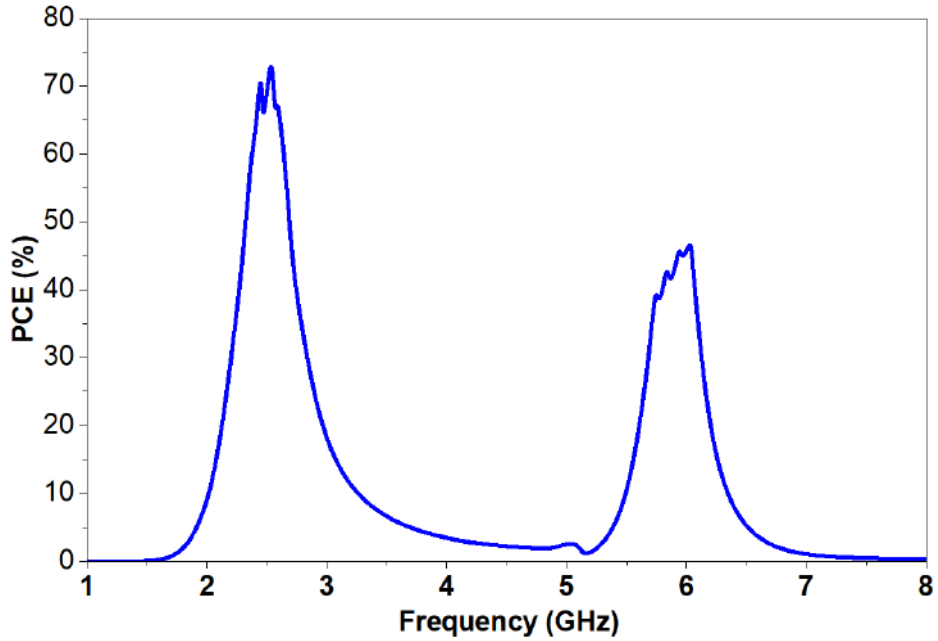

Figure 4.5: Power conversion efficiency of the dual-band rectifier for 2.45/5.8 GHz

In Figure 4.5, the simulated power conversion efficiency as a function of frequency is depicted, covering the 2.45/5.8 GHz Wi-Fi applications. The maximum conversion efficiency at 2.4 GHz is found as 73%. The maximum power conversion efficiency for the frequency of 5.8 GHz is found as 45%. Therefore, high PCE values and good matching of the dual-band rectifier

are obtained for both frequencies of 2.45 GHz and 5.8 GHz.

4.6 Performance comparison with the literature

The most important parameter in RFEH systems is the power conversion efficiency (PCE), which measures the ratio between DC-power at the load and AC-power available at the source. Table 4.1 compares the proposed rectenna with those proposed in the literature. The proposed rectifier shows the highest PCE compared to the works presented in [4–6, 34].

Table 4.1: Comparison with literature

Ref. year	Wi-Fi band (GHz)	P_{in} (dBm)	PCE (%)
[4], 2023	5.8	20	42.56 %
[5], 2024	2.4/5	0	52.64 %
[6], 2025	2.4/5.8	10	34 %
[34], 2022	2.45/5.8	10	66 %
Proposed	2.45/5.8	5	73%

4.7 Conclusion

In this chapter, we have designed a dual-band RF rectifier for Wi-Fi energy harvesting applications. We have used an L-section matching network for each band to match the source to the voltage doubler rectifier. High PCE values of 73% and 45% have been respectively achieved at 2.45 GHz and 5.8 GHz. Also, peak DC output voltages of 2.43 V and 2 V have been obtained at 2.45 GHz and 5.8 GHz, respectively.

General Conclusion

This work has been organized and structured into four chapters, progressing from theoretical foundations to practical implementation and focusing on the design of an antenna and an RF energy harvesting rectifier for 2.45 GHz and 5.8 GHz Wi-Fi applications.

In first chapter, general concepts related to antennas have been introduced, including their fundamental role as the interface between electromagnetic waves and electrical currents. Also, key antenna parameters such as gain, efficiency, polarization, and bandwidth have been presented and discussed, providing the necessary theoretical background. Then, in the second chapter, we focused on the theoretical aspects of RF energy harvesting, analyzing the feasibility of utilizing ambient RF sources such as Wi-Fi and cellular signals. The operation of a rectenna and its main components, including an antenna, impedance matching network, and rectifier circuit have been explained. Factors affecting harvesting efficiency, such as radiation losses, impedance mismatch, and circuit losses, have been carefully examined.

In the third chapter, simulation results of a dual-band antenna for Wi-Fi applications covering 2.45 GHz and 5.8 GHz has been presented and discussed. The proposed antenna demonstrated excellent performance over the operating bands, with acceptable realized gain values of 1.73 dBi at 2.45 GHz and 5.9 dBi at 5.8 GHz, and high radiation efficiencies of 83.23% and 91.16%, respectively. These results confirm that the antenna is highly suitable for dual-band Wi-Fi energy harvesting applications.

In the fourth chapter, the associated RF energy harvesting rectifier circuit has been designed. An L-section matching network has been used for each band to interface the antenna with a voltage doubler rectifier. The rectifier achieved high power conversion efficiencies (PCE) of 73% at 2.45 GHz and 45% at 5.8 GHz, with peak DC output voltages of 2.43 V and 2 V at 2.45 GHz and 5.8 GHz, respectively. These outcomes emphasize the importance of integrating an optimized antenna design with a precisely matched rectifier circuit to achieve high performance RF energy harvesting. In summary, this work provides a practical contribution to the field of self-sustaining RF energy harvesting systems, paving the way for future improvements in antenna structures and rectifier topologies.

Bibliography

[1] W. A. Serdijn, A. L. R. Mansano, and M. Stoopman, "Introduction to rf energy harvesting," in *Wearable Sensors*, pp. 299–322, Elsevier, 2014.

[2] A. Belhedri, B. Mekimah, B. Hammache, T. A. Denidni, A. Messai, and M. Boulesbaa, "High efficiency, low-power rf energy harvesting tri-band rectenna for mid-band 5g and wi-fi 6e applications," *Applied Computational Electromagnetics Society Journal (ACES)*, vol. 41, no. 5, 2026.

[3] R. Visintini, "Rectifiers," *CAS-CERN Accelerator School: Specialised CAS Course on Power Converters*, pp. 133–184, 2006.

[4] I. Salhane, M. Rifi, H. Terchoune, and S. Elmorabeti, "5.8 ghz rectenna for wireless powering battery-less sensors," in *ITM Web of Conferences*, vol. 52, p. 03005, EDP Sciences, 2023.

[5] L. Prashad, H. C. Mohanta, and A. J. Abdullah Al-Gburi, "Dual band rectenna for electromagnetic energy harvesting at 2.4 ghz and 5 ghz frequencies.," *Progress In Electromagnetics Research B*, vol. 108, 2024.

[6] O. Assogba, A. K. Mbodji, A. K. Farota, A. K. Diallo, A. Bréard, and Y. Duroc, "Dual-band rectifier dedicated to 2.45 and 5.8 ghz bands for radiofrequency energy harvesting," *Microwave and Optical Technology Letters*, vol. 67, no. 2, p. e70138, 2025.

[7] C. A. Balanis, *Antenna theory: analysis and design*. John wiley & sons, 2016.

[8] W. L. Stutzman and G. A. Thiele, *Antenna Theory and Design*. John Wiley & Sons, 3rd ed., 2012.

[9] S. Weiss, "Fundamentals on antennas and antenna definitions," *NATO Science and Technology Organization*, 2025.

[10] B. Mekimah, A. Messai, and T. Djerafi, *Amélioration des caractéristiques des patchs microbandes pour les applications ultra large bande*. PhD thesis, Université Frères Mentouri-Constantine 1, 2020.

[11] S. A. Ahson and M. Ilyas, *RFID handbook: applications, technology, security, and privacy*. CRC press, 2017.

[12] B. Mekimah, A. Messai, and A. Belhedri, "Gain enhancement of a cpw-fed dipole antenna using a novel multiband planar artificial magnetic conductor surface for uwb applications," *International Journal of Wireless and Mobile Computing*, vol. 21, no. 2, pp. 141–152, 2021.

[13] B. Mekimah, T. Djerafi, A. Messai, and A. Belhedri, "A reconfigurable antenna in frequency band and radiation using active frequency selective surfaces on the basis of pin diodes," in *2021 IEEE Microwave Theory and Techniques in Wireless Communications (MTTW)*, pp. 238–242, IEEE, 2021.

[14] B. Mekimah, T. Djerafi, A. Messai, and A. Belhedri, "A reconfigurable multi-band antenna with a high selectivity in frequency on the basis of pin diodes," in *2022 19th International Multi-Conference on Systems, Signals & Devices (SSD)*, pp. 2074–2077, IEEE, 2022.

[15] B. Mekimah, A. Messai, and A. Belhedri, "Analysis of the effect of dielectric losses on the bandwidth of microstrip patch antenna in stacked geometry and modelling," *SN Applied Sciences*, vol. 2, no. 4, p. 767, 2020.

[16] B. Mekimah, A. Messai, S. Aris, M. A. Meriche, and T. Fortaki, "The effect of the loss tangent on the bandwidth of the microstrip antennas in stacked configuration," in *Proceedings of 2014 mediterranean microwave symposium (MMS2014)*, pp. 1–5, IEEE, 2014.

[17] L. Boccia and O. Breinbjerg, "Antenna basics," *Space Antenna Handbook*, pp. 1–35, 2012.

[18] B. Mekimah, T. Djerafi, A. Messai, and A. Belhedri, "Broadband circularly polarized cpw-fed asymmetrically-shaped slot patch antenna for x band applications," *Progress In Electromagnetics Research Letters*, vol. 91, pp. 137–143, 2020.

[19] B. Mekimah, M. Abderraouf, M. A. Meriche, and A. Belhedri, "Miniaturized and circularly polarized inverted c shaped patch antenna for

x and ku bands applications," in *2018 18th Mediterranean Microwave Symposium (MMS)*, pp. 361–364, IEEE, 2018.

[20] B. Mekimah, T. Djerafi, A. Messai, A. Belhedri, M. Boulesbaa, and A. Hamidi, "Circularly polarized square loop shaped passive rfid transponder for thin uhf applications in random mobility use," in *2023 Workshop on Microwave Theory and Technology in Wireless Communications (MTTW)*, pp. 144–148, IEEE, 2023.

[21] A. Hamidi, B. Mekimah, S. Berhab, T. Djerafi, A. Belhedri, and M. Boulesbaa, "A high gain circularly polarized passive rfid tag on a metallic reflector for uhf band applications," in *2024 8th International Conference on Image and Signal Processing and their Applications (ISPA)*, pp. 1–4, IEEE, 2024.

[22] D. M. Pozar, *Microwave Engineering*. John Wiley & Sons, 4th ed., 2012.

[23] I. Singh, V. Tripathi, *et al.*, "Micro strip patch antenna and its applications: a survey," *Int. J. Comp. Tech. Appl*, vol. 2, no. 5, pp. 1595–1599, 2011.

[24] A. R. O. Mumin Warfaa, *Analysis of three different dielectric substrates on square ring microstrip antenna for wireless application*. PhD thesis, Universiti Tun Hussein Onn Malaysia, 2015.

[25] H. H. Ibrahim, M. J. Singh, S. S. Al-Bawri, S. K. Ibrahim, M. T. Islam, A. Alzamil, and M. S. Islam, "Radio frequency energy harvesting technologies: A comprehensive review on designing, methodologies, and potential applications," *Sensors*, vol. 22, no. 11, p. 4144, 2022.

[26] M. P. Aparicio, A. Bakkali, J. Pelegri-Sebastia, T. Sogorb, and V. Bou, "Radio frequency energy harvesting-sources and techniques," *Renew. Energy Util. Syst. Integr*, vol. 10, p. 61722, 2016.

[27] A. Nechibvute, A. Chawanda, N. Taruvinga, and P. Luhanga, "Radio frequency energy harvesting sources," *Acta Electrotechnica et Informatica*, vol. 17, no. 4, pp. 19–27, 2017.

[28] S. Almorabeti, M. Rifi, and H. Terchoune, "Rectifier circuit designs for rf energy harvesting applications," in *Colloque sur les Objets et systèmes Connectés*, 2019.

[29] S. N. Arinze, E. R. Obi, S. H. Ebenuwa, and A. O. Nwajana, "Rf energy-harvesting techniques: Applications, recent developments,

challenges, and future opportunities," in *Telecom*, vol. 6, p. 45, MDPI, 2025.

[30] C. Mikeka, H. Arai, *et al.*, "Design issues in radio frequency energy harvesting system," *Sustainable Energy Harvesting Technologies-Past, Present and Future*, pp. 235–256, 2011.

[31] F. Mbombolo and S. Eden, *Etude et conception d'une rectenna pour un transfert d'energie sans fil point a point par faisceaux micro-ondes*. Library and Archives Canada, Ottawa, 2013.

[32] V. Lavanya, C. Rimmya, S. Piramasubramanian, and M. M. Ganesh, "Review of microwave (rf) energy harvesting techniques," *IntechOpen*, 2025.

[33] K. Singh, S. Yadav, J. Deegwal, and M. Sharma, "Analysis of rf-dc rectifier input impedance for the appropriate design of matching network for wireless rf energy harvesters," *Wearable and Neuronic Antennas for Medical and Wireless Applications*, pp. 85–104, 2022.

[34] J. Li, Z. Li, C. Jiang, T. Wei, and Z. Liu, "Designing and modeling of a dual-band high-efficiency rectenna using dielectric resonant antenna array," *Applied Sciences*, vol. 12, no. 19, p. 10081, 2022.